Jupiter's X-rays 2007 Part 1: Jupiter's X-ray Emission During Solar Minimum

W. R. Dunn[1,2,3], G. Branduardi-Raymont[1,2], V. Carter-Cortez[1,2], A. Campbell[2], R. Elsner[4], J-U. Ness[5], G. R. Gladstone[6], P. Ford[7], Z. Yao[8], P. Rodriguez[5], G. Clark[9], C. Paranicas[9], A. Foster[3], D. Baker[1], R. Gray[10], S. V. Badman[10], L. C. Ray[10], E. J. Bunce [11], B. Snios[3], C. M. Jackman[12], I. J. Rae[1], R. Kraft[3], A. Rymer[9], S. Lathia[2], N. Achilleos[2]

[1]Mullard Space Science Laboratory, Department of Space & Climate Physics, University College London, Holmbury St. Mary, Dorking, Surrey RH5 6NT, UK
[2]The Centre for Planetary Science at UCL/Birkbeck, Gower Street, London, WC1E 6BT, UK
[3]Harvard-Smithsonian Center for Astrophysics, Smithsonian Astrophysical Observatory, Cambridge, 02138, MA, USA
[4]NASA Marshall Space Flight Center, Huntsville, Alabama, USA
[5]European Space Astronomy Centre, Madrid, Spain
[6]Space Science and Engineering Division, South West Research Institute, San Antonio, Texas, USA
[7]Kavli Institute of Astrophysics and Space Research, MIT, Cambridge, MA, USA
[8]Laboratoire de Physique Atmospherique et Planetaire, Universite de Liege, Liege, B-4000, Belgium
[9]The Johns Hopkins University Applied Physics Laboratory, Laurel, MD, USA
[10]Department of Physics, Lancaster University, Lancaster, LA1 4YW, UK
[11]Department of Physics and Astronomy, University of Leicester, Leicester, UK
[12]Department of Physics and Astronomy, University of Southampton, Southampton, SO17 1BJ, UK

Key Points:

- Jupiter's equatorial X-ray emission varies in accordance with solar cycle 24 but auroral power can be comparably bright at solar min & max
- Charge Exchange models provide good fits to aurora spectra retrieving S:O ratios of 0.4-1.3 agreeing with in-situ magnetosphere measurements
- We report systematic differences between Chandra ACIS and XMM-Newton EPIC-pn Jovian spectra and the impact of these on opacity and quenching

Corresponding author: William R Dunn, `w.dunn@ucl.ac.uk`

Abstract

The 2007-2009 solar minimum was the longest of the space age. We present the first of two companion papers on Chandra and XMM-Newton X-ray campaigns of Jupiter through February-March 2007. We find that low solar X-ray flux during solar minimum causes Jupiter's equatorial regions to be exceptionally X-ray dim (0.21GW at minimum; 0.76GW at maximum). While the Jovian equatorial emission varies with solar cycle, the aurorae have comparably bright intervals at solar minimum and maximum. We apply atomic charge exchange models to auroral spectra and find that iogenic plasma of sulphur and oxygen ions provides excellent fits for XMM-Newton observations. The fitted spectral S:O ratios of 0.4-1.3 are in good agreement with in-situ magnetospheric S:O measurements of 0.3-1.5, suggesting that the ions that produce Jupiter's X-ray aurora predominantly originate inside the magnetosphere. The aurorae were particularly bright on Feb 24-25 and March 8-9, but these two observations exhibit very different spatial, spectral and temporal behaviour. 24-25 Feb was the only observation in this campaign with significant hard X-ray bremsstrahlung from precipitating electrons, suggesting this may be rare. For 8-9 March, a bremsstrahlung component was absent, but bright oxygen O^{6+} lines and best-fit models containing carbon, point to contributions from solar wind ions. This contribution is absent in the other observations. Comparing simultaneous Chandra ACIS and XMM-Newton EPIC spectra showed that ACIS systematically under-reported 0.45-0.6keV Jovian emission, suggesting quenching may be less important for Jupiter's atmosphere than previously thought. We therefore recommend XMM-Newton for spectral analyses and quantifying opacity/quenching effects.

1 Introduction

With their launch in 1999, the XMM-Newton and Chandra X-ray Observatories ushered in a revolution in X-ray astronomy, providing a paradigm-shift in our understanding of Jupiter's X-ray (0.2 - 10 keV) emissions. The combination of these two complementary observatories have permitted an array of invaluable research on Jupiter's aurorae. So far, these studies have identified two dominant sources of Jupiter's X-ray emission: a) scattering and fluorescence of solar photons in Jupiter's atmosphere across the planet's Sun-lit face [*Branduardi-Raymont et al.*, 2004; *Bhardwaj et al.*, 2005, 2006; *Branduardi-Raymont et al.*, 2007a; *Cravens et al.*, 2006] and b) dynamic auroral emissions from the polar regions [*Gladstone et al.*, 2002; *Elsner et al.*, 2005; *Dunn et al.*, 2016, 2017; *Kimura et al.*, 2016]. Further, two distinct spectral components have been identified for the X-ray aurorae: hard X-ray (here considered as energy > 1.0 keV) electron bremsstrahlung aurorae [*Branduardi-Raymont et al.*, 2004, 2008] and soft X-ray ion spectral line aurorae (energies less than 1 keV) [*Elsner et al.*, 2005; *Branduardi-Raymont et al.*, 2007b; *Hui et al.*, 2010; *Dunn et al.*, 2016].

The hard X-ray aurorae are the lower latitude of these two aurorae. These emissions are the X-ray counterpart for the UV and IR main emission and are produced by $\sim$10-100 keV electrons [*Branduardi-Raymont et al.*, 2004, 2008]. In this location electrons precipitate along an upward current system that links Jupiter to its middle magnetosphere, imparting the planets angular momentum to the surrounding plasma in order to enforce corotation [e.g. *Cowley and Bunce* [2001]; *Hill* [2001]].

Poleward of the hard X-ray oval, there is the soft X-ray aurora which is dominated by charge exchange spectral lines that are produced when highly charged ions collide with Jupiter's atmosphere [*Cravens et al.*, 1995; *Kharchenko et al.*, 1998; *Gladstone et al.*, 2002; *Elsner et al.*, 2005; *Branduardi-Raymont et al.*, 2004, 2007b, 2008; *Kharchenko et al.*, 2006, 2008; *Ozak et al.*, 2010, 2013; *Dunn et al.*, 2016]. These ions precipitate from beyond 50 RJ (1 RJ = 1 Jupiter radius) [*Kimura et al.*, 2016; *Dunn et al.*, 2016, 2017] and are typically injected in pulses which sometimes have a regular pulsation rate but normally pulse erratically [*Gladstone et al.*, 2002; *Elsner et al.*, 2005; *Dunn et al.*, 2016, 2017; *Jackman* *et al.*, 2018]. A variety of processes have been proposed to explain these precipitations, including: downward currents that complete the upward corotation enforcement system [*Cravens et al.*, 2003], magnetopause processes such as reconnection [*Bunce et al.*, 2004] and/or Kelvin Helmholtz Instabilities [*Kimura et al.*, 2016; *Dunn et al.*, 2016, 2017], rotation-driven reconnection in the outer magnetosphere [*Guo et al.*, 2018a,b; *Yao et al.*, 2017] or a combination of wave processes [*Manners et al.*, 2018].

NASA's Juno mission has already provided several clues for how the ion precipitation and acceleration at Jupiter take place. Using the JEDI instrument's high energy ion data, *Clark et al.* [2017] have shown the presence of significant inverted-V structures in the data, which are often thought to characterise potential drops accelerating particles. *Paranicas et al.* [2018] have shown that MeV electrons stream out of the 'swirl region' in the polar cap of Jupiter, suggesting a significant source of acceleration within a few Jupiter radii of the planet's pole. *Haggerty et al.* [2017] detected in-situ ion precipitation during a Juno perijove, which may relate to the ion X-ray spectral line emissions that have been observed from the aurora for the last two decades [e.g. *Elsner et al.* [2005]; *Branduardi-Raymont et al.* [2004, 2007b]; *Hui et al.* [2010]].

To produce X-ray spectral lines from charge exchange requires the ions to be in particularly high charge states. Oxygen ions (O^{6+} and O^{7+}) have been found to be an excellent fit to Jupiter's auroral spectra [*Elsner et al.*, 2005; *Branduardi-Raymont et al.*, 2007b; *Hui et al.*, 2010]. Alongside the oxygen emission, there are many spectral lines from less energetic photons between 0.2-0.5 keV, where sulphur or carbon emission would dominate. Unfortunately, the spectral resolution of current instruments is insufficient to unambiguously distinguish between spectral lines from sulphur or carbon. Sulphur would suggest a magnetospheric origin for the X-ray emission, since Jupiter's magnetosphere is dominated by sulphur and oxygen ions that are injected by the volcanic moon Io. Instead, carbon would suggest a solar wind origin where the dominant heavy ions are oxygen and carbon [*Von Steiger et al.*, 2000]. In modelling the Chandra ACIS spectrum, *Elsner et al.* [2005] found that sulphur produced far better fits, but they could not conclusively rule-out carbon. *Branduardi-Raymont et al.* [2004, 2007b] found that for XMM-Newton spectra from 2003 typically sulphur produced better fits, but that there were some intervals where carbon could also provide a suitable fit. *Hui et al.* [2009, 2010] support this assessment when re-fitting these XMM-Newton and Chandra ACIS spectra pre-2007 and report that sulphur and oxygen provide a better fit for all but one observation, where carbon and oxygen was preferred.

While oxygen lines are always present in the auroral spectrum, some observations have suggested unusual ratios between the fluxes of these oxygen lines. From cometary charge exchange studies and theoretical models of line emission, O^{6+} emission is expected to peak between 0.55 - 0.6 keV [e.g. *Kharchenko and Dalgarno* [2000]; *Kharchenko et al.* [2003]; *Smith et al.* [2012]]. However, Jovian auroral observations by Chandra ACIS show very low levels of emission in this energy range and instead the oxygen emission peaked above 0.6 keV [e.g. *Elsner et al.* [2005]; *Dunn et al.* [2016]]. *Kharchenko et al.* [2008] showed that in order to attain good fits to the Chandra Jupiter data it is necessary to suppress the contribution from the otherwise dominant 0.561 keV O^{6+} forbidden transition originating from a long-lived metastable state. *Kharchenko et al.* [2008] explain that for acceleration into Jupiter's atmosphere, oxygen ions may undergo collisions within such a short timescale that oxygen dissipates energy before it has time to emit the 0.561 keV photon. This 'quenching' of the line by short timescale collisions would be efficient for altitudes below 1200 km, where the atmospheric density exceeds $10^{10} cm^{-3}$. *Ozak et al.* [2010, 2013] extended the Monte Carlo models of *Kharchenko et al.* [2008] and *Hui et al.* [2009, 2010] to include a variety of factors such as opacity, air glow, secondary electron fluxes and an atmospheric depth dependence of the emission. The extent of the opacity effects had to be tailored to account for the reduced 0.56-0.6 keV oxygen emission in the Chandra spectra.

However, the lack of detection of a 0.561 keV line in the Chandra ACIS Jovian spectra is contradicted by the XMM-Newton spectra, where emission between 0.55-0.58 keV is the dominant component [*Branduardi-Raymont et al.*, 2004, 2007b; *Hui et al.*, 2010]. It is therefore important to understand the differences between the Chandra and XMM-Newton Jovian spectra in order to correctly interpret the ion precipitations.

Here, we present the first in a series of 2 papers analysing the rich and diverse data available for Jupiter between February and March 2007. In this paper we focus on the general trends in the X-ray emissions from both the Jovian equatorial regions and the aurora during solar minimum. The second paper in the series [*Dunn et al.*, in review] compares the variability in the X-ray emissions with solar wind conditions, as measured by the New Horizons spacecraft, and with contemporaneous Hubble UV and Nançay and WIND radio observations. There is also a third paper in preparation which analyses in detail the multi-waveband auroral features that are triggered by various solar wind events and proposes physical processes that could produce them [Gray et al. in prep].

For this paper, we begin by introducing the X-ray observations (section 2). We then compare the disk emission during the 2007 solar minimum with observations during the solar cycle 24 maximum (2011 and 2014) and the declining phase (2016) (section 3). We follow this with analysis of the auroral spectra (section 4) and compare the Chandra ACIS and XMM-Newton Jovian auroral spectra to elucidate whether the variation in the oxygen lines are temporal or instrumental. We then fit these spectra using AtomDB atomic charge exchange spectral lines [*Smith et al.*, 2012] to identify the relative abundances of precipitating ions and to compare how these vary between observations and instruments. Finally, we utilise the Chandra ACIS spatial resolution in concert with its spectral and temporal resolution to probe the spatial distribution of the different precipitating species (section 5). We close by discussing these results and concluding (section 6 and 7).

2 Chandra and XMM-Newton X-ray Campaign

Between February and March 2007 a series of Jupiter X-ray observations were conducted with both Chandra's ACIS (Advanced CCD Imaging Spectrometer) instrument and with XMM-Newton's suite of EPIC-pn (European Photon Imaging Camera with pn CCDs), MOS (Metal Oxide Semi-conductor) and RGS (Reflection Grating Spectrometers) instruments. The ACIS instrument on the Chandra X-ray observatory offers good temporal (each exposure is 3.2 seconds long with a 42 ms readout time) and spatial resolution (0.5") and provides moderate spectral resolution ($\frac{E}{\Delta E}$ of 10-50). Since 2011, a contaminant build-up on the ACIS optical blocking filter has significantly reduced the viability of the instrument for Jupiter observations, so the observations analysed here represent a rare opportunity for simultaneous spatial, spectral and temporal resolution. XMM-Newton provides limited spatial resolution (5"), but better spectral resolution ($\frac{E}{\Delta E}$ of 10-50 for EPIC or 100-500 for RGS), time resolution (photons time-tagged with an accuracy of 0.03ms) and sensitivity (collecting area almost an order of magnitude larger than Chandra's - see supporting information). We note that Chandra ACIS and EPIC-pn typically detect between 0 and 10 (with a mean of 1 to 2) counts per minute from Jupiter's aurorae, but $\sim$100 counts are needed to begin effective modelling of the Jovian spectra. With current instrument sensitivity, a Jovian X-ray aurora spectrum is therefore limited to an integration over several hours of auroral visibility, when the aurorae are known to be dynamic over timescales of minutes.

The X-ray observations were shorter than other Jovian X-ray campaigns covering ~ 0.5 Jupiter rotations each. At the time of the observations, Jupiter's sub-observer latitude was -3.31°, so observations slightly favoured the Southern jovigraphic pole and limited visibility of the Northern geographic pole. The observation times and associated longitude range are listed in Table 1. Jupiter's aurorae rotate with the planet and thus are generally confined to a certain Jupiter-centred (S3) latitude and longitude range. The

Observatory	ID	Start - End Time	DoY	CML Start - End	Aurora in View
CXO	7405	8 Feb 08:31 - 13:47	39	94°-286°	N
CXO	8216	10 Feb 19:54 - 11 Feb 01:21	41-42	88°-286°	N
CXO	8217	24 Feb 21:24 - 25 Feb 02:17	55-56	90°-267°	N
XMM	0413780101	24 Feb 20:14 - 25 Feb 03:02	55-56	47°-294°	N
CXO	8219	3 Mar 07:43 - 13:03	62	286°-120°	S
XMM	0413780201	3 Mar 07:17 - 14:42	62	271°-180°	S
CXO	8220	7 Mar 14:19 - 19:08	66	48°-223°	Both
XMM	0413780301	7 Mar 12:52 - 20:21	66	356°-267°	Both
CXO	8218	8 Mar 21:04 - 9 Mar 02:45	67-68	83°-290°	N
XMM	0413780401	8 Mar 19:50 - 9 Mar 02:20	67-68	39°-275°	N

Table 1. The observation IDs; start and end times; corresponding Central Meridian Longitude (CML) visibility and consequent visible aurora for each Chandra (CXO) ACIS and XMM-Newton (XMM) observation in 2007. Details for non-2007 observations can be found in the supporting information.

dipole tilt and asymmetric magnetic field mean that the auroral longitude locations and morphology are different for each pole. For the North, the aurorae are more strongly offset from the spin axis and are mostly situated between ∼140-270° S3 longitude and above 55° latitude. The Southern aurorae are more closely aligned to the spin axis, but still feature an offset with a viewing preference from ∼300-120° S3 longitude and above 60° latitude [e.g. Dunn et al. 2017 and Fig 9 and 10 here]. Table 1 shows that the observations on 8th, 10th and 24-25th February and 8-9th March provided coverage of the Northern aurora, while 3rd March covered the Southern aurora and 7th March covered the transition between the two. For all Chandra observations red light contamination ('red-leak') through the ACIS Optical Blocking Filter was accounted for in the manner described in *Elsner et al.* [2005].

Compared with previous X-ray observations, the combination of the shorter observation duration and large Jupiter-Earth distances (5.28 AU) meant that the measured X-ray photon counts were below average [e.g. *Jackman et al.* [2018]]. This lead the observations by XMM-Newton's EPIC-MOS and RGS instruments to have a very low signal for these observations. EPIC-pn's effective area at 0.5 keV through a thick filter (used to prevent contamination from visible emission) is ∼550 cm^2, compared with ∼120 cm^2 for each EPIC-MOS module and ∼50 cm^2 for each RGS module. For these low signal observations our use of XMM-Newton focuses on the EPIC-pn instrument, since the signal was exceptionally low for the other instruments. Although we do note that Chandra and XMM-Newton produce very few spurious events and Jupiter blocks the cosmic X-ray background, so the noise is very low (particularly for Chandra's high spatial resolution).

3 Jovian Equatorial Emission During Solar Minimum

Figure 1 shows that all previous Jupiter observations by Chandra and XMM-Newton in the X-ray literature occurred during solar maximum or the declining phase of the solar cycle. In contrast, these 2007 observations (alongside the ROSAT 1995 [*Gladstone et al.*, 1998] observations) occured during solar minimum.

One of the most striking aspects of the 2007 X-rays observations of Jupiter is that the only identifiable emission from the planet is the polar aurora. Figure 2 shows that during solar maximum, the planet provided a clearly defined disk of emission, but for solar minimum in 2007 the equator is barely discernible from the background. The CML

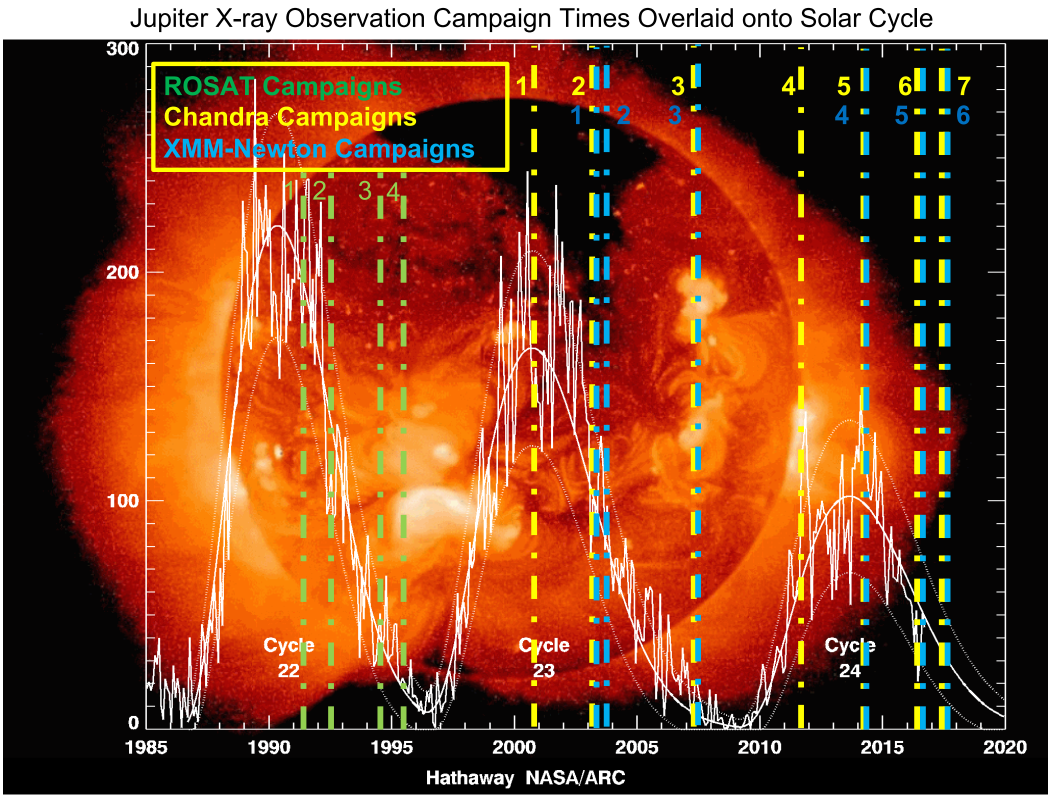

Figure 1. Times of ROSAT (green), Chandra (yellow) and XMM-Newton (blue) observing campaigns of Jupiter pre-2018 as dash-dotted lines overlaid on a NASA/ARC solar cycle graphic [credit: Hathaway] showing sunspot number through the last 3 decades. The publications relating to each are ROSAT 1&2: *Waite et al.* [1994] 3: *Waite et al.* [1995, 1997] 4: *Gladstone et al.* [1998]. Chandra: 1: *Gladstone et al.* [2002]; 2: *Elsner et al.* [2005]; *Bhardwaj et al.* [2006]; *Branduardi-Raymont et al.* [2008]; *Hui et al.* [2009, 2010]; *Ozak et al.* [2010]; 3: This paper; *Dunn et al.* [in review]; 4: *Dunn et al.* [2016] 5: *Kimura et al.* [2016] 6: *Dunn et al.* [2017] 7: Gladstone et al. [in prep]. *Jackman et al.* [2018] summarise X-ray periodicity from 1999-2015. XMM-Newton: 1: *Branduardi-Raymont et al.* [2004] 2: *Branduardi-Raymont et al.* [2007b,a]; *Bhardwaj et al.* [2005]; *Hui et al.* [2010] 3: This paper; *Dunn et al.* [in review] 4: *Kimura et al.* [2016] 5: *Dunn et al.* [2017] 6: Dunn et al. [in prep].

range for these images permitted viewing of the Northern but not the Southern aurora. *Bhardwaj et al.* [2005, 2006]; *Cravens et al.* [2006]; *Branduardi-Raymont et al.* [2007a] show that the emission from Jupiter's equatorial region is largely dependent on the solar X-ray output, which is known to vary with the solar cycle.

3.1 Equatorial Spectra

Spectra were extracted and calibrated using the standard procedures with the Chandra CIAO or XMM-Newton SAS software and then grouped to meet the needs of fitting with XSPEC [*Arnaud*, 1996], while applying the appropriate response files [e.g. Branduardi-Raymont et al. 2004; Dunn et al. 2016]. Firstly, we contrast the XMM-Newton EPIC-pn equatorial spectra from 3 observations chosen to represent different points in the solar cycle: 2007 (solar minimum), 2014 (solar maximum) and 2016 (declining phase). Figure 3a shows representative images of the Sun from Hinode's XRT [*Golub et al.*, 2008] at each point in the solar cycle showing the proliferation of activity and flaring regions moving from minimum in 2007 to maximum in 2014 and then their decline through May 2016. Figure 3b shows the X-ray irradiance measured by the GOES spacecraft for each observation showing that for 2007 (blue) the X-ray irradiance in the 0.05-0.4 nm (3-25 keV) and 0.1-0.8nm (1.5-12 keV) bands were at the limits of detection for the spacecraft with irradiances 3 orders of magnitude less than during solar maximum in 2014 (yellow) and 1-2 orders of magnitude less than during the declining phase in 2016 (green). The energy ranges that we fit the equatorial spectra from are 0.2-1.5 keV which reveal variation in the Sun's X-ray emission in a lower energy regime than GOES is capable of observing.

The limited spatial resolution of XMM-Newton leads some auroral emission to contaminate the equatorial region [e.g. Branduardi-Raymont et al. 2004]. When selecting the spectrum we chose a region centred on the equator with conservative latitudinal extent to minimise this (see supporting information for region selection). For 2007, each observation had a similar count-rate from the equatorial region. In Fig 3c, we present spectra from 3 March because the CML range of this observation led it to provide the least auroral contamination into the equatorial region. Figure 3c shows the equatorial spectrum from 3 March 2007 (solar minimum - in blue), 15 April 2014 (solar maximum - in yellow) and 24 May 2016 (declining phase - in green) overlaid.

Each EPIC-pn equatorial spectrum was fitted with an APEC model (Astrophysical Plasma Emission Code) [*Smith et al.*, 2001], which produces a collisionally-ionised diffuse gas emission spectrum from temperature, normalisation and atomic composition parameters. Solar abundances were chosen in order to represent the solar corona. We attained best fit models with reduced χ^2 of 0.5 - 1.3 (for Jovian X-ray aurora, a reduced $\chi^2 > 1.5$ typically shows a poor fit) for each spectrum and measured the photon fluxes from these model fits between 0.2-1.5 keV (beyond 1.5 keV the flux diminishes to near zero). Due to the relatively low number of counts for the 2007 observations, the data were grouped into energy channel bins with at least 5 counts, rather than the 10 normally used in XSPEC fitting. For consistency, this was applied in the modelling of all three observations. Figures 4a, b and c show the best-fit theoretical APEC models (upper panels) and the models convolved with the instrument response and overlaid on the spectral data points (lower panels).

We quote the fluxes as measured from integrating under the spectrum (Fig 4) observed at Earth orbit and the powers are calculated accounting for the Jupiter-Earth distance, which for 2007, 2014 and 2016 were 5.28, 4.7 and 4.34 AU respectively. For solar minimum in 2007, maximum in 2014 and declining phase in 2016 we measure fluxes of photons/cm^2/s (powers) of: 1.4 x 10^{-5} (0.21 GW), 5.1 x 10^{-5} (0.76 GW) and 1.8 x 10^{-5} (0.23 GW) respectively. For comparison with previous measurements we used $4\pi r^2$

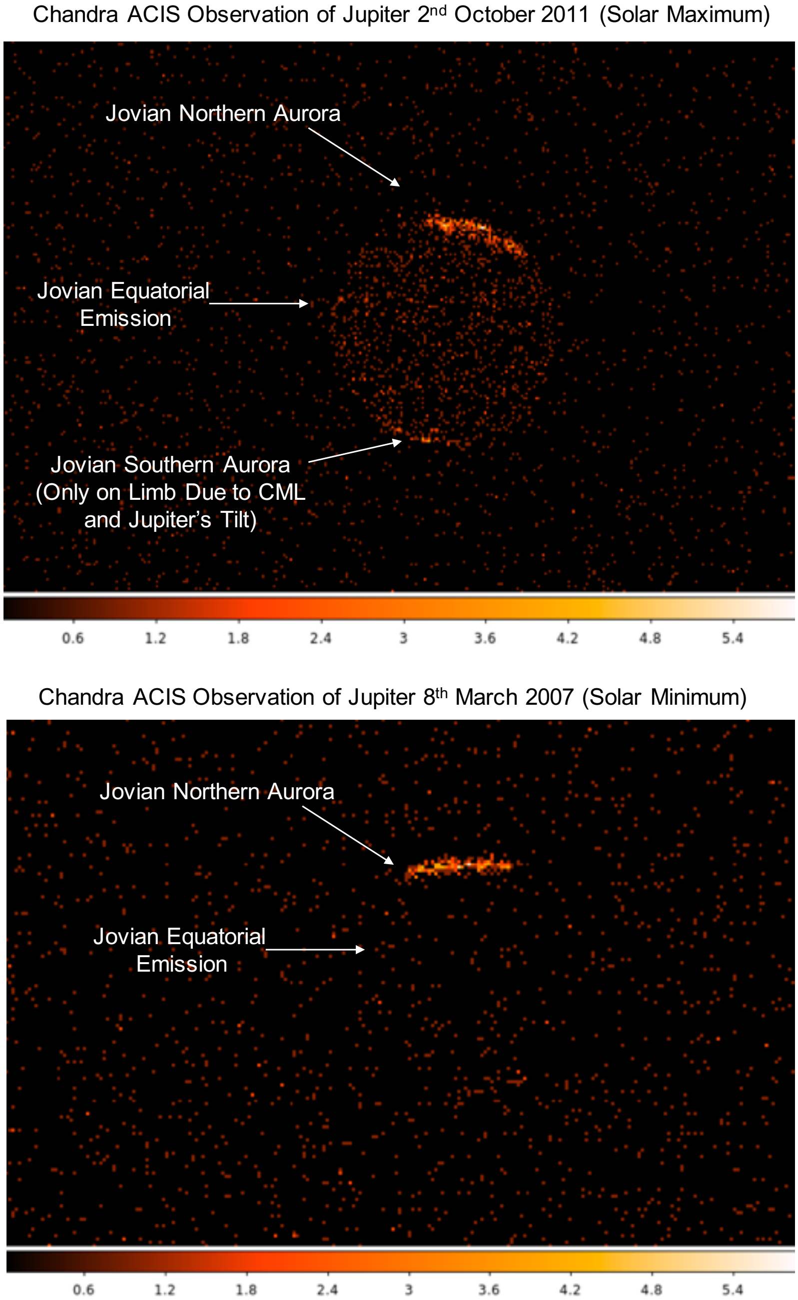

Figure 2. Two Chandra ACIS Images of Jupiter each covering a 5.7 hour integration across the CML range 83°-290°. On October 2nd 2011 (upper), Jupiter was exposed to X-rays from the Sun at solar maximum and the entire of Jupiter is clearly distinguished from the background (equator count rate: 0.03 counts/sec), through these scattered solar photons from the entire disk [*Bhardwaj et al.*, 2005, 2006; *Cravens et al.*, 2006; *Branduardi-Raymont et al.*, 2007a]. In contrast, for March 8-9th 2007 (lower), the Sun was at solar minimum and it is very difficult to distinguish a defined planetary disk (equator count rate: 0.004 counts/sec) but Jupiter's Northern aurora is distinguishable from the background (Jupiter's disk blocks background X-ray emission). We note that the Southern aurora is just discernible on the limb of Jupiter's South pole for the 2011 observation. The CML range means that the majority of the Southern aurora would have been on the side of Jupiter that faced away from the Earth at this time, but the slight tilt of the planet's pole relative to Earth, means that a fraction of this emission appears on the limb. In 2011, Jupiter was at 4.07 AU, while in 2007 it was at 5.27 AU. Spectra from the equatorial regions during different phases of solar activity are fitted and scaled for the distance to provide power estimates in the main text.

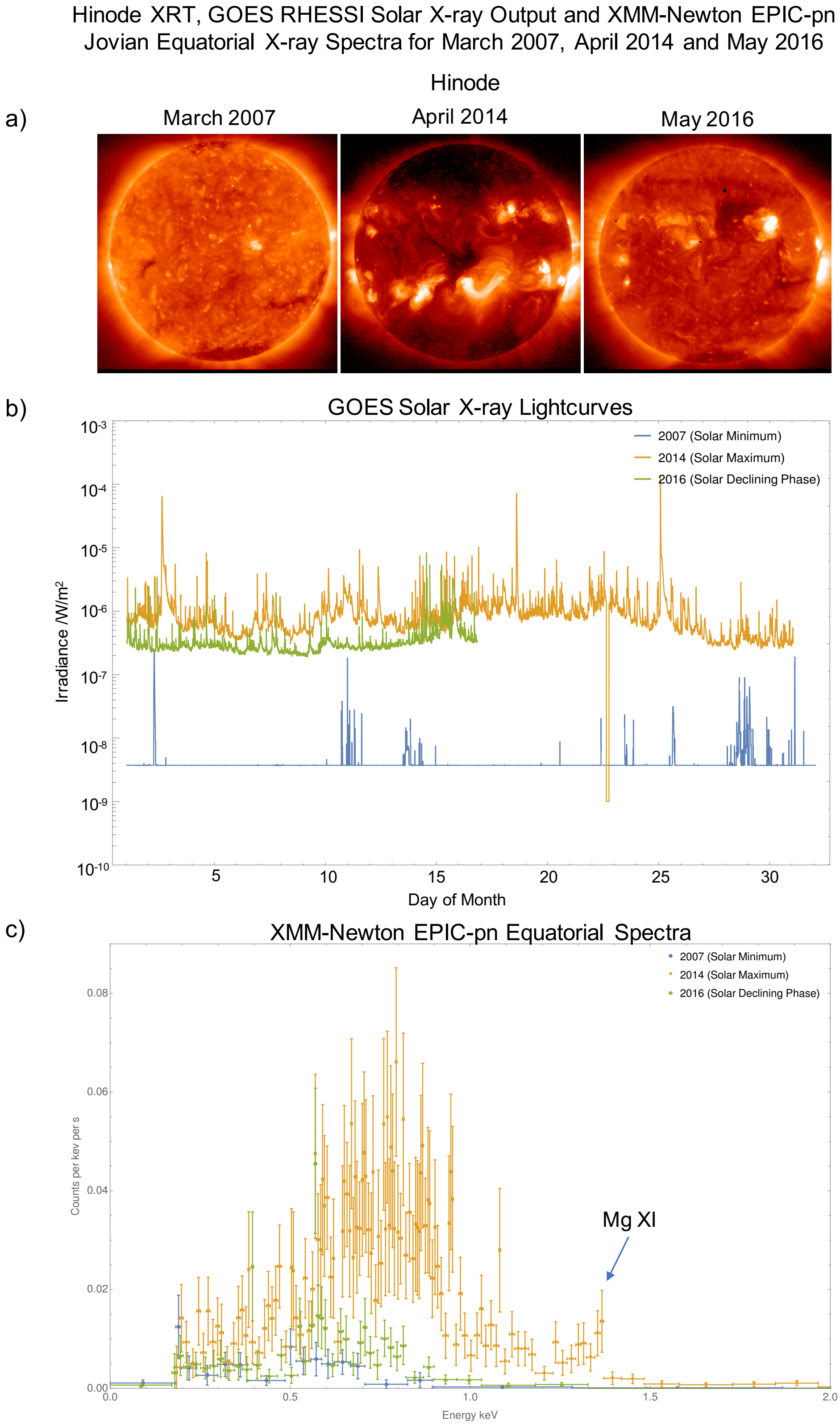

Figure 3. a) Hinode XRT (0.2-3 keV) Images of the Sun on 15th March 2007 (filter: Al-Mesh); 24th April 2014 (filter: Ti-Poly); 26 May 2016 (filter: Al-Mesh). The Ti-Poly filter was used during April 2014 because it has a lower response to the high coronal temperatures present during solar maximum [*Golub et al.*, 2008]. This filter highlights the high-luminosity flares and prominences on the Sun at this time, which are far less prevalent in 2007 and 2016. b) GOES measurements of solar X-ray irradiance between 0.05-0.4 nm (3-25 keV) plotted against day of month for March 2007, April 2014 and May 2016 - during solar minimum, maximum and declining phase respectively c) X-ray spectra from Jupiter's equatorial region for 3 March 2007, 15 April 2014 and 24 May 2016.

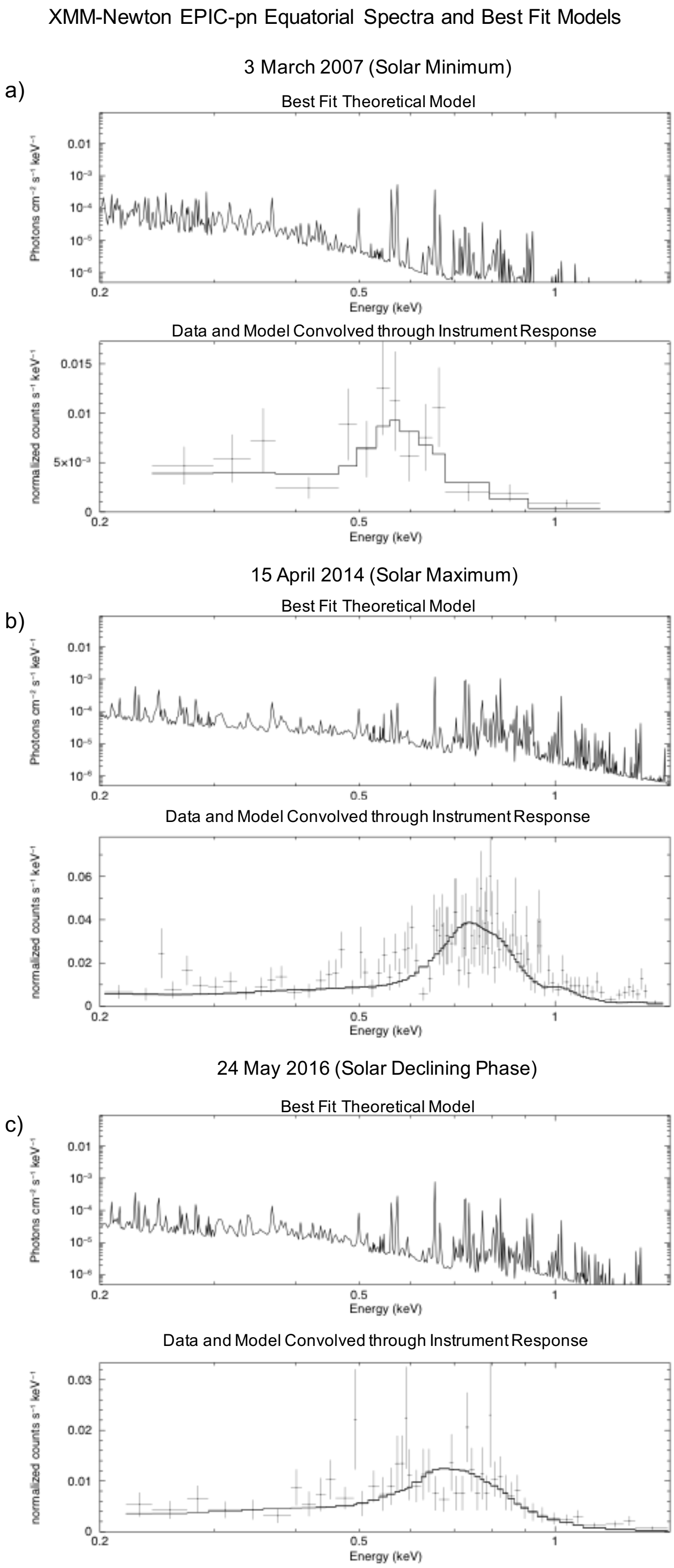

Figure 4. Jovian Equatorial Spectra from a) the 3rd March 2007 during the pre-solar cycle 24 Solar Minimum b) the 15th April 2014 during Solar Maximum of cycle 24 and c) the 24 May 2016 during the declining phase of solar cycle 24. Upper panels show best fit theoretical models using an APEC solar corona model. Lower panels show this model convolved with the instrument response (black line) and overlaid on the XMM-Newton EPIC-pn Jupiter equatorial spectrum (crosses).

to calculate the disk power, but note that because only one side of Jupiter is Sun-lit, $2\pi r^2$ may be more appropriate.

Our results show that the order of magnitude changes in X-ray irradiance measured by GOES lead to changes of a factor of 4 in the power output from Jupiter's disk. This discrepancy between the power measured by GOES and that measured from the Jovian equator could be due to a combination of the different wavelength ranges of the two instruments (3-25 keV for GOES vs 0.2-2 keV for EPIC-pn) and Jupiter's energy-dependent X-ray albedo [*Cravens et al.*, 2006].

Alongside changes in the equatorial emission power, the model fits reveal changes in the solar corona temperature across the solar cycle with the Jovian equatorial spectra from 2007 (solar minimum), 2014 (solar maximum) and 2016 (declining phase) being best fit by coronal models with a kT of 0.18±0.02 keV, 0.42±0.02 keV and 0.29±0.02 keV respectively. Figure 3c and 4 show this variability in the data and that the peak of the spectrum shifts to higher energies during solar maximum. Since the Mg XI lines between 1.3-1.4 keV are only seen at solar maximum these may track significant solar heating. However, we note that the observed equatorial emissions are a convolution of the solar spectrum with absorption, scattering and fluorescence from the Jovian atmosphere. This means that the deduced coronal temperatures are relative values and not a true solar coronal temperature.

4 Auroral Spectra

The low levels of scattered solar emission mean that the 2007 observations provide the cleanest X-ray aurora observations recorded. Figure 2 clearly shows variability in the disk emission between solar minimum and solar maximum, however an auroral variation is less clear. While 372 ± 19 Northern Aurora X-ray counts were detected in the 83°-290° CML range for October 2nd 2011 (a particularly bright observation - *Dunn et al.* [2016]), only 239±15 Northern auroral photons were found in 2007 from the same CML range (for both a 5.7 hour integration). However, Jupiter was only 4.07 AU from the Earth in Oct 2011, but was 5.28 AU away in Feb-March 2007. When this distance difference is accounted for, these two observations represent comparable auroral outputs of ∼2 GW (assuming a $4\pi r^2$ scaling), with 8th March 2007 being moderately more powerful. At first glance, year-to-year variability [e.g. *Jackman et al.* [2018]] appears to link to solar cycle, however changes in Jupiter-Earth distance may account for much of this.

4.1 Comparing Chandra ACIS with XMM-Newton EPIC Spectra

The 2007 observations represent a unique opportunity to directly compare simultaneous Jovian aurora spectra from XMM-Newton and Chandra ACIS to better understand the previously reported differences that are outlined in the introduction and highly relevant for Monte Carlo ion precipitation models for Jupiter's aurora [e.g. *Kharchenko et al.* [2008]; *Ozak et al.* [2010]; *Hui et al.* [2009, 2010]]. Figure 5 shows the 4 simultaneous (trimmed to identical time windows) Chandra ACIS and XMM-Newton EPIC-pn Northern aurora spectra from: 24-25 Feb and 7, 8-9 March and Southern auroral spectrum from 3 March.

Comparing the Chandra ACIS and XMM-Newton EPIC-pn spectra shows that there are systematic differences between the two. Chandra ACIS under-detected Jovian emission in certain regions of the spectrum (particularly 0.45-0.6 keV) relative to XMM-Newton EPIC-pn and MOS. Alternatively, there is a ∼ 30-50 eV shift to higher energies in the Chandra spectrum relative to the EPIC-pn spectrum. Figure 5 shows that XMM-Newton EPIC-pn auroral spectra consistently peak at the 0.55-0.59 keV O VII lines, but for Chandra the peak is instead between 0.6 - 0.7 keV. Below 0.5 keV there are also significant differences. ACIS S3 CCD, used for all Jovian observations, is uncalibrated below ∼ 400

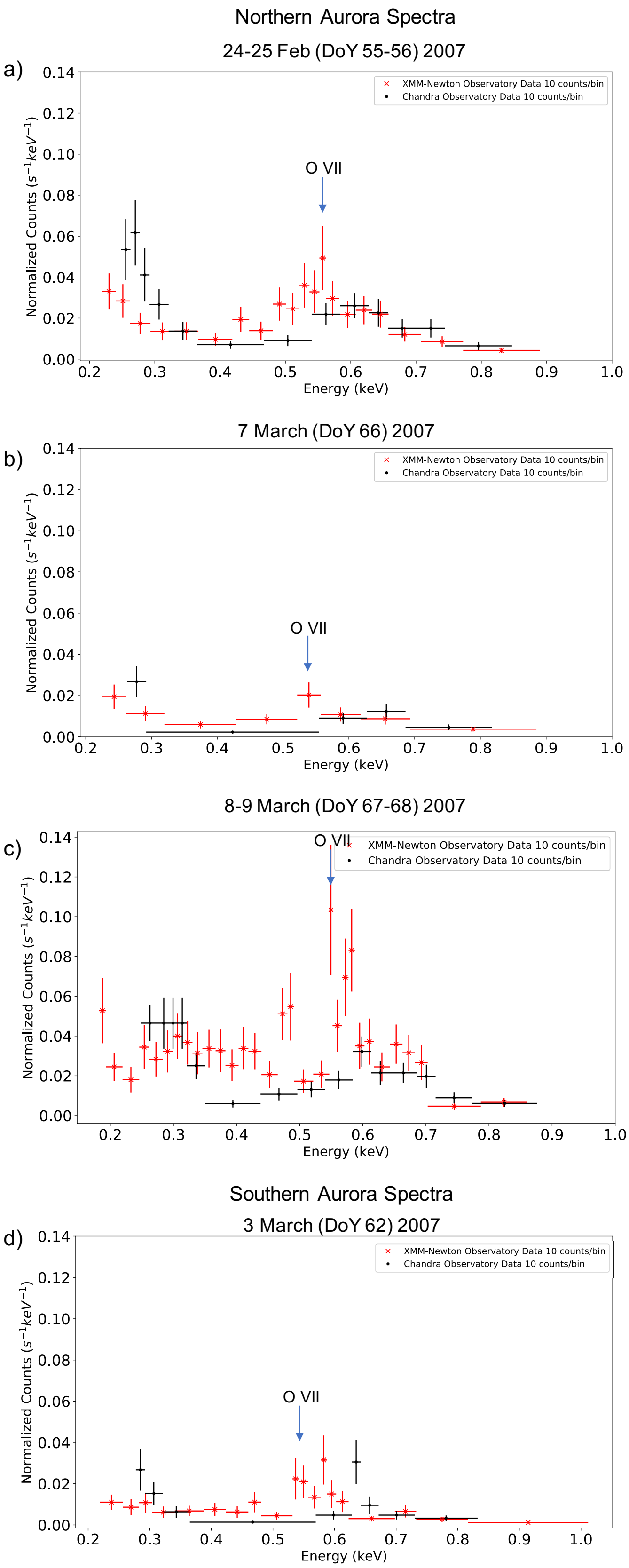

Figure 5. Comparison of the Chandra ACIS (black) and XMM-Newton EPIC-pn (red) Northern auroral X-ray spectra for a) the 24th Feb 2007, b) the 7th and c) 8th March 2007 and d) Southern auroral X-ray spectrum for 3 March 2007. Arrows indicate the location of the O VII charge exchange emission lines at 0.55-0.59 keV.

eV and the contaminant that has subsequently built-up on the optical blocking filters contains significant abundances of carbon, so even in 2007 these may have contributed noise and/or signatures around the carbon k-edge (0.28 keV). For reference and comparison with previous work (e.g. Ozak et al. 2010; Hui et al. 2010), we show fits of the spectrum in this region to show that Chandra ACIS fits always prefer a sulphur auroral population, however, we emphasise that the Jovian ACIS spectra below 0.4 keV should not be interpreted for spectral line analysis and the reasons previously listed are accentuated by unrealistic photon fluxes (e.g. Fig 7 and Table 2). While the spectral emissions are poorly resolved, the spatial distribution of 0.2-0.5 keV photons is similar to the oxygen emission and in the locations reported for previous X-ray observations (e.g. Fig 9 and *Gladstone et al.* [2002]). This suggests that the detections are real, but that poor constraints on the instrument effective area at low energies limits interpretation of the spectrum.

Based on this, we caution consideration of the relative energy-responses for both instruments for interpretation of the auroral data. In all previous observations [e.g. *Branduardi-Raymont et al.* [2007b], XMM-Newton EPIC-pn measures 0.561 keV emission closer to the expected laboratory and theoretical/modelled values [e.g. *Kharchenko and Dalgarno* [2000]; *Kharchenko et al.* [2003]; *Smith et al.* [2012]], we therefore use EPIC-pn as the more reliable instrument for scientific interpretation of the auroral spectra for the remainder of the paper.

4.2 Fitting Jupiter's Spectra with Atomic Charge Exchange Models

Alongside instrumental trends, Figure 5 reveals the auroral variation from observation to observation. The 7th of March provided the longest and most complete CML coverage of the Northern aurora in 2007 and yet the emission is the dimmest. The oxygen emission is most notably bright for 8-9 March, with a prominent peak at the ∼0.56 keV oxygen line and a clear unusual bump in emission between 0.4-0.5 keV. The 24-25 Feb observation has the only noteworthy hard (greater than 1 keV) X-ray emission of the campaign and a clear oxygen peak, although this is less bright than the 8-9 of March.

Comprehensive gaussian line analyses have been previously conducted on Jovian auroral spectra previously [e.g. *Elsner et al.* [2005]; *Branduardi-Raymont et al.* [2004, 2007b]; *Dunn et al.* [2016]]. Given the low energy resolution of the CCD spectra, we pursued a self-consistent approach on a physical basis, exploring the precipitating particle populations through AtomDB (http://www.atomdb.org/) charge exchange spectral line lists [*Smith et al.*, 2012, 2014].

The models offer a possible alternative to the Monte Carlo Models used to simulate the whole process of ion precipitation, charge stripping, charge exchange, atmospheric absorption and subsequent photon yields (Examples detailed in *Kharchenko et al.* [2006, 2008]; *Ozak et al.* [2010]; *Hui et al.* [2009, 2010]). Instead, a theoretical model is produced from a given abundance and a charge state distribution of the precipitating ions is determined by a thermal, kT, energy (the atmosphere these collide with is assumed to be cold and neutral). From this, a line spectrum is calculated and the quality of its fit to the data is determined. We then iterate through different possible abundances and temperatures, testing the fit of each of their subsequent line spectra until a best-fit is identified by minimising a reduced χ^2. We note that a temperature parameter for a thermalised plasma will not comprehensively represent the non-thermal collisional processes that produce the X-ray aurora in the manner that can be accomplished by monte carlo models for ion precipitation such as those shown in *Kharchenko et al.* [2006, 2008]; *Ozak et al.* [2010]; *Houston et al.* [2018]. We instead use this as an 'equivalent temperature' to provide a diagnostic of the charge state distribution and therefore to observationally and semi-quantitatively track the acceleration that Jupiter applies to the precipitating ions from observation to observation. We assumed the Jovian atmosphere to be 10% Helium

Instrument	Date	ACX Model	χ^2 of fit	kT (keV)	CX Flux (ph/cm^2/s)	S:O or C:O
XMM EPIC-pn	24-25 Feb	S+O	0.8	0.18±0.01	2±0.2 x 10^{-6}	0.7
CXO ACIS	24-25 Feb	S+O	0.9	0.1±0.01	5±2 x 10^{-4}	1.9
XMM EPIC-pn	24-25 Feb	C+O	1.3	0.18±0.01	2.0±0.2 x 10^{-6}	0.4
CXO ACIS	24-25 Feb	C+O	8	0.2±0.1	3±2 x 10^{-4}	1.7
XMM EPIC-pn	8-9 March	S+O	1.3	0.25±0.04	2±1 x 10^{-6}	1.24
CXO ACIS	8-9 March	S+O	3	0.2±0.1	8±7 x 10^{-4}	1.9
XMM EPIC-pn	8-9 March	C+O	1.1	0.20±0.01	3.5±0.5 x 10^{-6}	1
CXO ACIS	8-9 March	C+O	4	0.19±0.01	5±4 x 10^{-4}	1.3

Table 2. Best-fit Parameters for S+O and C+O atomic charge exchange model fits to the XMM-Newton (XMM) EPIC-pn and Chandra (CXO) ACIS Northern Auroral Spectra. This shows for each instrument, observation and model: the χ^2 of the best fit model, the temperature of the ion distribution (diagnostic of their charge state distribution and thereby energy), the photon fluxes produced from ion charge exchange and the ratio of S:O or C:O. We note that the Chandra ACIS instrument response has an uncertain calibration below 0.4 keV and also a contaminant build-up on the optical blocking filters which leads to potentially unrealistic photon fluxes.

and 90% Hydrogen in accordance with measurements, and with few charge exchange line lists available for ion collisions with Jovian atmospheric hydrocarbons. The AtomDB Atomic charge exchange lines were able to produce excellent fits to almost every XMM-Newton data set (reduced χ^2 of 0.8-1.3), although the required ion temperature (charge state distribution), abundance and photon flux parameters for each fit varied from observation to observation. Figure 6 provides an example of the sulphur lines produced at a given temperature, showing how the location of spectral lines varies for each given charge state of sulphur.

The models provide a useful metric for qualitatively tracking the energy of the precipitating ions (Fig 6). Given enough energy, when an ion collides with the atmosphere it will have electrons stripped from it. Ions with higher energies will have more electrons stripped [e.g. *Ozak et al.* [2010]]. The charge states of ions therefore provide a way to track the acceleration of the ion population. For instance, the presence of S^{10+} spectral lines suggests more energy was available for collisional electron stripping than if these lines were absent and only e.g. S^{9+}, S^{8+} and S^{7+} lines were observed. Different charge states of an ion will produce photons with different energies. Figure 6 shows the energies and emissivities at which different charge states of sulphur produce photons: clearly higher charge states populate higher energy regimes in the soft X-ray spectrum. It is therefore possible to track energisation of the precipitating ions through the charge states of lines observed.

The number of photons produced during charge exchange depends on a complex array of factors including: the precipitating ion populations, the local atmosphere conditions (e.g. temperature, density and composition) the charge exchange cross sections from the combination of these factors and also stochastic processes such as the transition probability of certain spectral lines. The atomic charge exchange models presented here provide a valuable tool for disentangling the photon fluxes from the charge state distributions, and thereby help provide qualitative constraints on the energy of the precipitating ions.

In applying this model we tested a range of possible physical processes for the generation of spectral lines for the Chandra ACIS and XMM-Newton EPIC-pn data. We

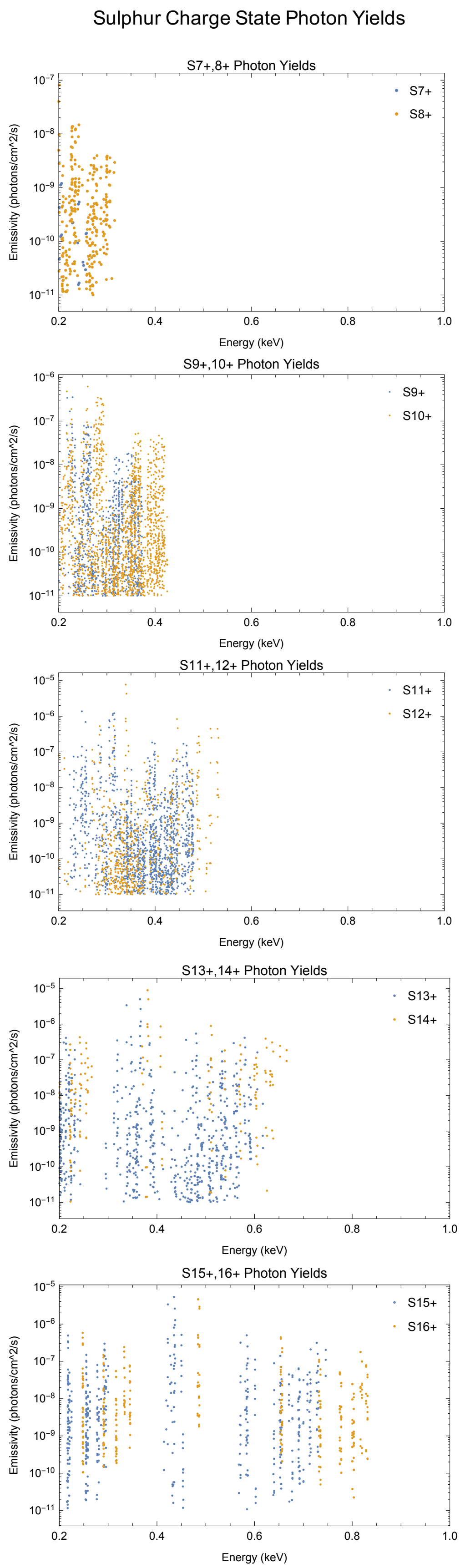

Figure 6. Atomic Charge Exchange Model Flux Photon Yields of Sulphur show that higher charge states dominate higher energy regions of the spectrum. These higher charge states are produced when the energy of the ion population is increased. Higher charge state emissions therefore indicate more energetic ion precipitations. These theoretical spectra therefore help auroral spectra observers to constrain the energies of the precipitating ions. Model parameters in supporting information.

tested two cases for the charge state distribution. The first case was a solar wind-like interaction, in which the ions only charge exchange once during the interaction (the charge state distribution is held constant), we herein refer to this case as the Single Charge eXchange model (SCX). The second case was a Multiple Charge eXchange (MCX) case, where an ion charge exchanges through each successive charge state until it is neutral (the charge state distribution changes with each charge exchange process). We note that many of these transitions occur at energies below those detected by XMM-Newton or ACIS, and instead produce EUV photons. A SCX model may better represent an atmosphere that becomes opaque to emission, since as the ions precipitate deeper they will undergo progressively more charge exchange interactions but the emission lines from these lower charge states are more likely to be absorbed by the atmosphere.

Typically, the SCX model fits were slightly worse than MCX, with marginal increases on the reduced χ^2 of ~ 0.1 for all datasets (despite maintaining the same number of free parameters). While the fits were similar, an SCX model required that the S:O abundance ratio increased by up to a factor of 2. This is because between 0.2-0.5 keV there are spectral lines from charges states of S6+ to S13+. If a single ion can transition from S^{13+} through S^{12+}, S^{11+}, S^{10+}, S^{9+}, S^{8+} and S^{7+} on route to S^{6+}, then fewer sulphur ions would be needed to produce the observed emission. In contrast, oxygen only has X-ray lines from O^{7+} to O^{5+} between 0.5-0.9 keV. If each ion only produced one observed charge exchange line, then one would require an increased S:O ratio to explain the broader range of emissions from sulphur charge states than oxygen states.

4.3 Identifying the Precipitating Ion Population

Our goal was to further explore the discussion of an oxygen-sulphur population against an oxygen-carbon population, which is less favoured through theoretical arguments (e.g. *Cravens et al.* [2003]; *Bunce et al.* [2004]) and previous spectral fits [*Elsner et al.*, 2005; *Branduardi-Raymont et al.*, 2007b; *Hui et al.*, 2009, 2010]. For brevity, in this paper we therefore consider only models that fit populations containing oxygen, sulphur and/or carbon, but more complete ion models are shown in the companion paper [*Dunn et al.*, in review].

For both the Chandra and XMM-Newton spectra we found that we could obtain good fits (reduced $\chi^2 \sim 1-1.5$) to most datasets from models that only used sulphur and oxygen ions. We tried forcing fits with specific abundances and also tried fitting for specific parameters of: oxygen abundance, sulphur abundance and energy of the population (charge state distribution through a thermalised plasma temperature). If we set initial conditions for the model to contain small abundances of oxygen and sulphur (e.g. 0.1 of the solar photosphere abundance), the resulting fits would always favour models that raised the sulphur abundances by 1-2 orders of magnitude. The best fit sulphur:oxygen (S:O) ion ratios that we retrieved were surprisingly close to Jovian magnetospheric populations (see section 6.3). A typical sulphur and oxygen charge exchange model is shown fitted to the February 24th Northern aurora observation in Figure 7a - this model had a reduced χ^2 fit of 0.8 to the XMM Newton EPIC-pn spectrum and was best fit by an S:O ratio of 0.7 for an ion multiple charge exchange model and 1.3 for a single charge exchange model.

Either sulphur or carbon can explain the emission from 0.3-0.4 keV. However, below 0.27 keV there are no notable carbon lines. Figure 7b shows a best fit for a purely oxygen and carbon model and highlights the key difference between the two model fits: spectra that have a raised flux between 0.2-0.28 keV will always be fitted better by a sulphur population, which produces a forest of low charge-state emission in this region (see Fig. 6). This trend is accentuated for the ACIS spectra shown in Figure 7c and d where a sulphur+oxygen model is clearly favoured over a carbon+oxygen model (reduced χ^2 > 6). However, the instrument response for ACIS has an uncertain calibration below

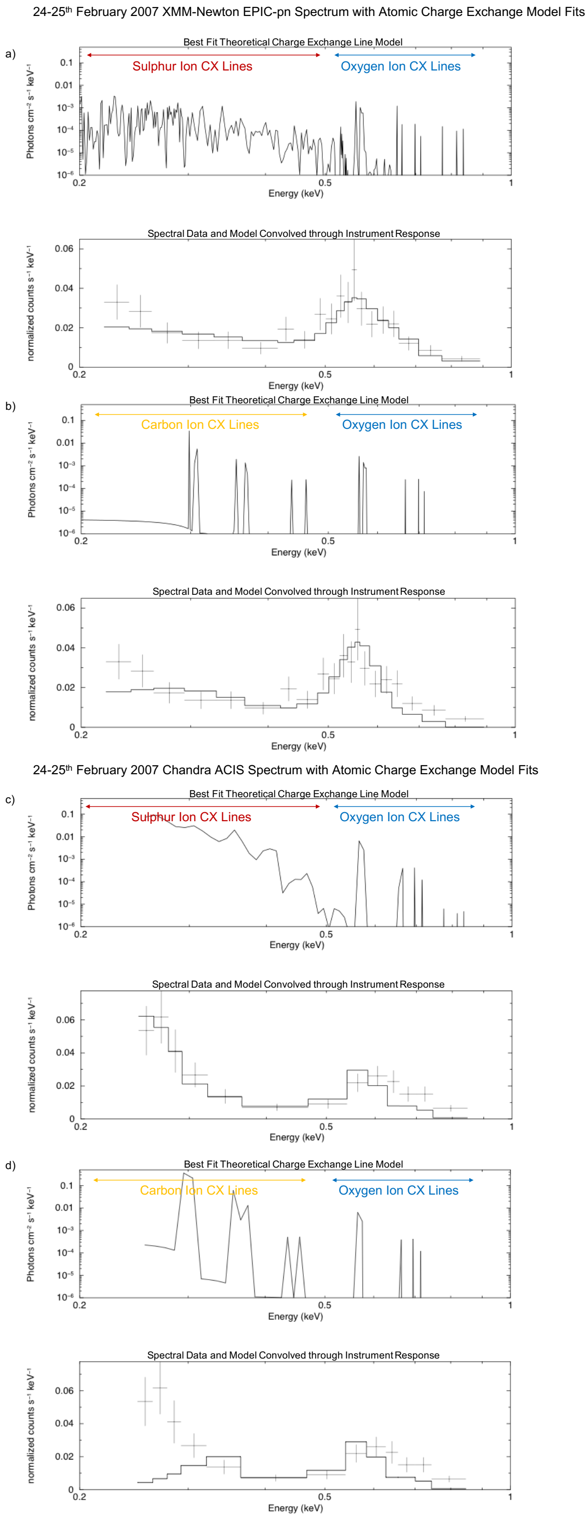

488 **Figure 7.** 24-25th February 2007 Northern Aurora Spectrum: XMM-Newton EPIC-pn data
489 with theoretical charge exchange models for a) sulphur and oxygen ions , b) carbon and oxygen
490 ions. Chandra ACIS spectral data with theoretical charge exchange models for c) sulphur and
491 oxygen ions, d) carbon and oxygen ions. Upper panels respectively are the best fit theoretical
492 atomic charge exchange models of sulphur+oxygen or carbon+oxygen ions and assume that each
493 ion charge exchanges multiple times to produce several spectral lines. Lower panels respectively
494 are the models convolved through the instrument response (black line) and plotted with the
495 XMM-Newton EPIC-pn or Chandra ACIS data (crosses). See Table 2 for model parameters.

0.4 keV, and includes a build-up of contaminant on the optical blocking filters. For this reason, model fits should not be extended below 0.4 keV and the impact of these poor constraints on spectral fits at low energies is shown in Table 2 and Fig. 7 and 8.

The previously discussed diminished Chandra ACIS 0.55-0.6 keV emission (*Kharchenko et al.* [2008]) is again observed in Figure 8c and d, where, after the instrument responses are accounted for, the oxygen charge exchange peaks between 0.55-0.59 keV (Fig. 5) are a factor of 2-5 higher for EPIC-pn than for ACIS (also present in 7). However, the key difference is that the ACIS spectra peak at a higher energy than the XMM spectra. This leads to significant changes in the best fit model parameters (see Table 2). This inability to reproduce the emission observed in the Chandra ACIS spectra leads to best fits with reduced χ^2 of 2.7-4. The differing calibrations below 0.6 keV lead the best-fit charge exchange models to require very different parameters for ACIS and EPIC-pn (see Table 2). The XMM-Newton EPIC-pn spectrum instead shows a clear peak in the oxygen emission at 0.57-0.6 keV that was well reproduced by charge exchange models (reduced χ^2 of 1.1-1.3). In fact, the opposite may be true for EPIC-pn spectrum: the model underestimates the 0.55-0.59 keV oxygen emission.

While sulphur and oxygen charge exchange models provided good fits for most Chandra ACIS and XMM-Newton EPIC-pn spectra, these were not without exception. Figure 8a shows a purely sulphur and oxygen charge exchange model fit to the 8th March 2007 EPIC-pn spectrum, which achieves a good reduced χ^2 fit of 1.3. However, the reduced emission from 0.2-0.3 keV and peaked emission between 0.4-0.5 keV is actually a better fit to a purely carbon and oxygen charge exchange model as shown in Figure 8b, which provided a reduced χ^2 fit of 1.1 (Table 2). *Hui et al.* [2009, 2010] noted the importance of a spectral feature between 0.425 and 0.475 keV for distinguishing carbon from sulphur.

5 Chandra ACIS Observations Polar Projections

Chandra ACIS provides spatial, spectral and temporal resolution, which allows us to compare the spatial origins of emission from differing precipitating particle populations. To do this, we re-registered the X-ray photons to the System III (S3) latitude-longitude positions from which they originate (as shown in *Gladstone et al.* [2002]; *Elsner et al.* [2005]; *Branduardi-Raymont et al.* [2008]; *Dunn et al.* [2016, 2017]). Figures 9 and 10 show S3 latitude-longitude X-ray 'heat maps' showing the density of X-ray photons centred on the Northern Pole and Southern Pole (see supporting information for photon polar projections). While we note previously that Chandra produces discrepancies for spectral line fitting, the spatial resolution is irreplaceable for studying the auroral morphology for different precipitating particle populations. To study species-dependent spatial distributions the projections are divided as 0.2-0.5 keV sulphur/carbon ion line emission (in red), 0.5-0.9 keV oxygen ion line emission (in blue) and above 1 keV hard X-ray bremsstrahlung from electron precipitation (in green-yellow) for all of the 2007 observations combined. The maps show that the 0.2-1 keV X-ray emission is concentrated poleward of the UV main emission and has the densest concentration in the UV active region, but there is some distribution further poleward of this. The hard X-ray emission occurs both along the main emission and includes emission poleward of this. The variability and spatial distribution of the hard X-rays is explored in detail in *Dunn et al.* [in review].

6 Results and Discussion

6.1 Disk Emission

The X-ray emission from Jupiter's Sun-lit face was very dim throughout the 2007 campaign (Figure 2). The APEC model of collisionally-ionised emission from a diffuse gas of solar composition provided good fits to the equatorial spectrum throughout dif-

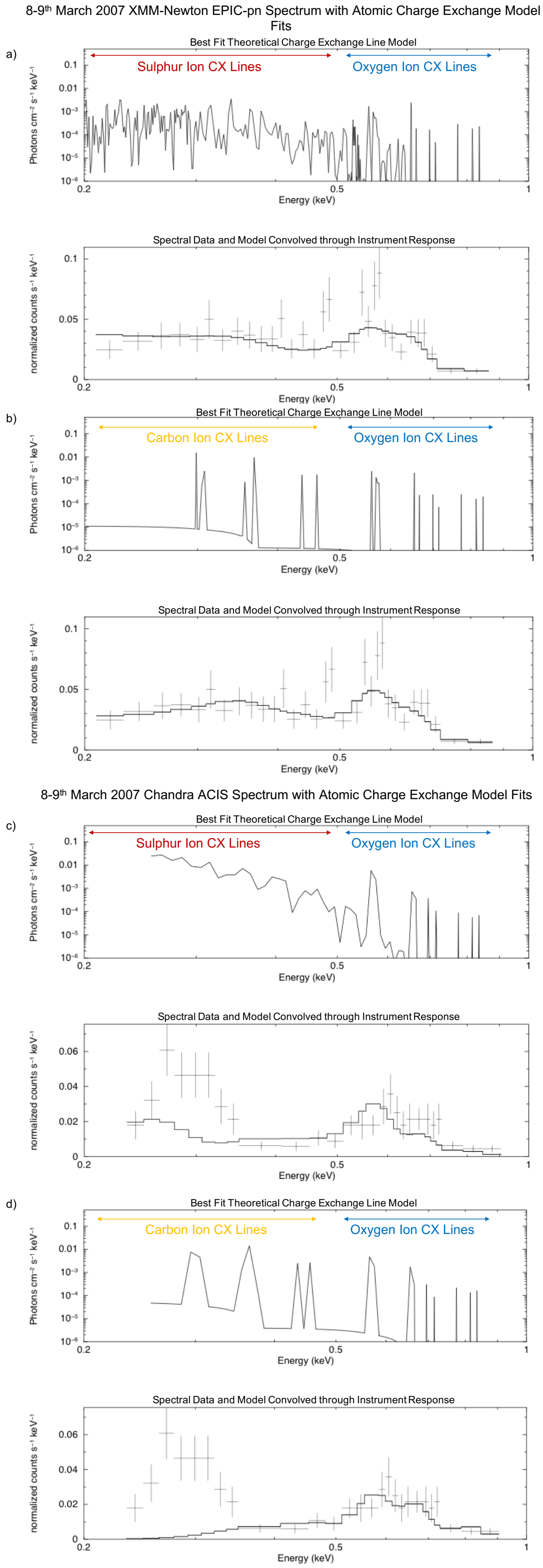

521 **Figure 8.** Same as Figure 7 but for 8-9th March 2007. See Table 2 for model parameters.

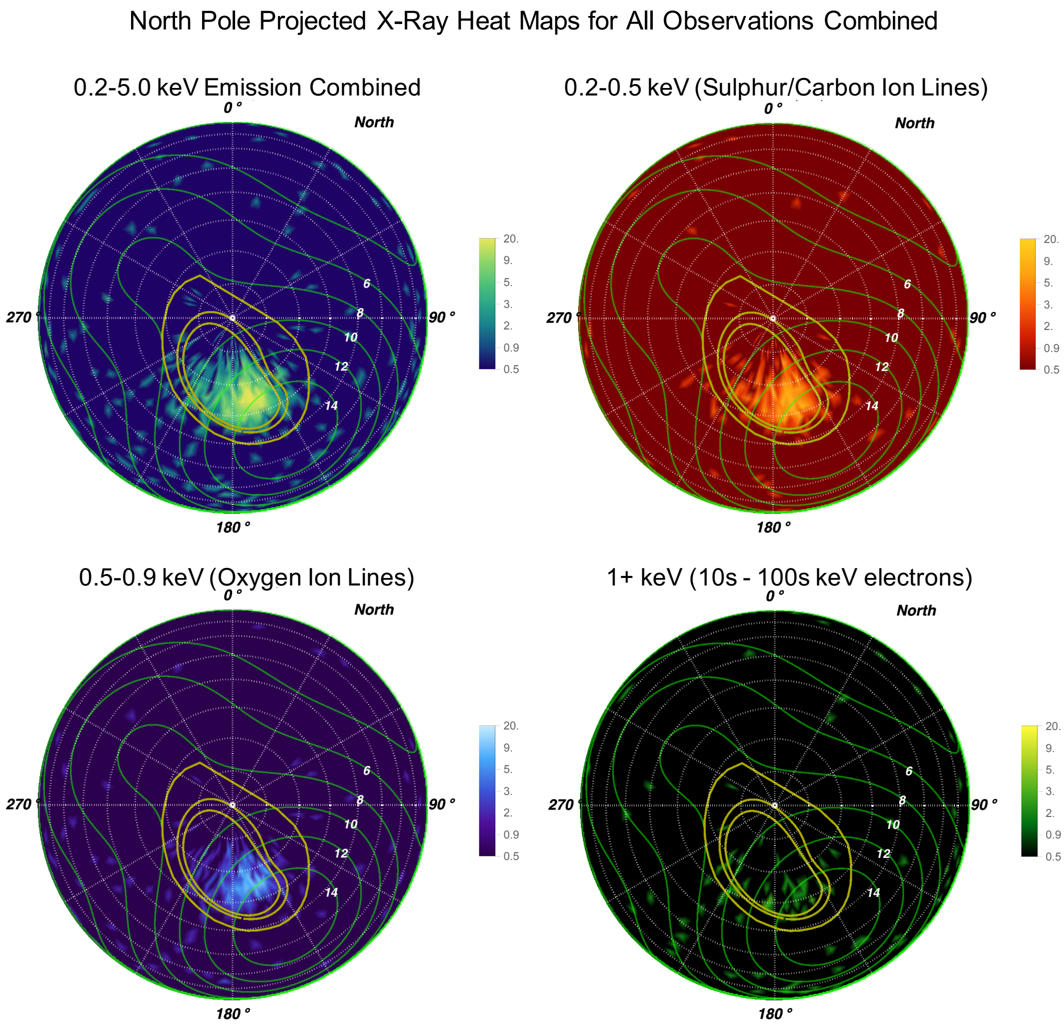

Figure 9. Projected X-ray heat maps centred on Jupiter's North pole from Chandra ACIS observations. These show a) the full energy range in blue-green-yellow b) 0.2-0.5 keV (sulphur/carbon emission) in red-yellow c) 0.5-0.9 keV (oxygen emission) in blue-white and d) greater than 1 keV emission (hard X-ray bremsstrahlung from electron precipitation) in green-yellow. The logarithmic colour bar indicates the number of X-rays in bins of 3° by 3° of S3 latitude-longitude. Dashed grey lines of longitude radiate from the pole, increasing clockwise in increments of 30° from 0° at the top. Concentric grey dotted circles outward from the pole represent lines of latitude in increments of 10°. Thin green contours with white text labels indicate the VIP4 [*Connerney et al.*, 1998] model magnetic field strength in Gauss. Thick gold contours show the magnetic field ionospheric footprints of field lines intersecting the Jovigraphic equator at 5.9 RJ (Io's orbit), 15 RJ and 45 RJ [*Grodent et al.*, 2008; *Vogt et al.*, 2011, 2015] from equator to pole respectively.

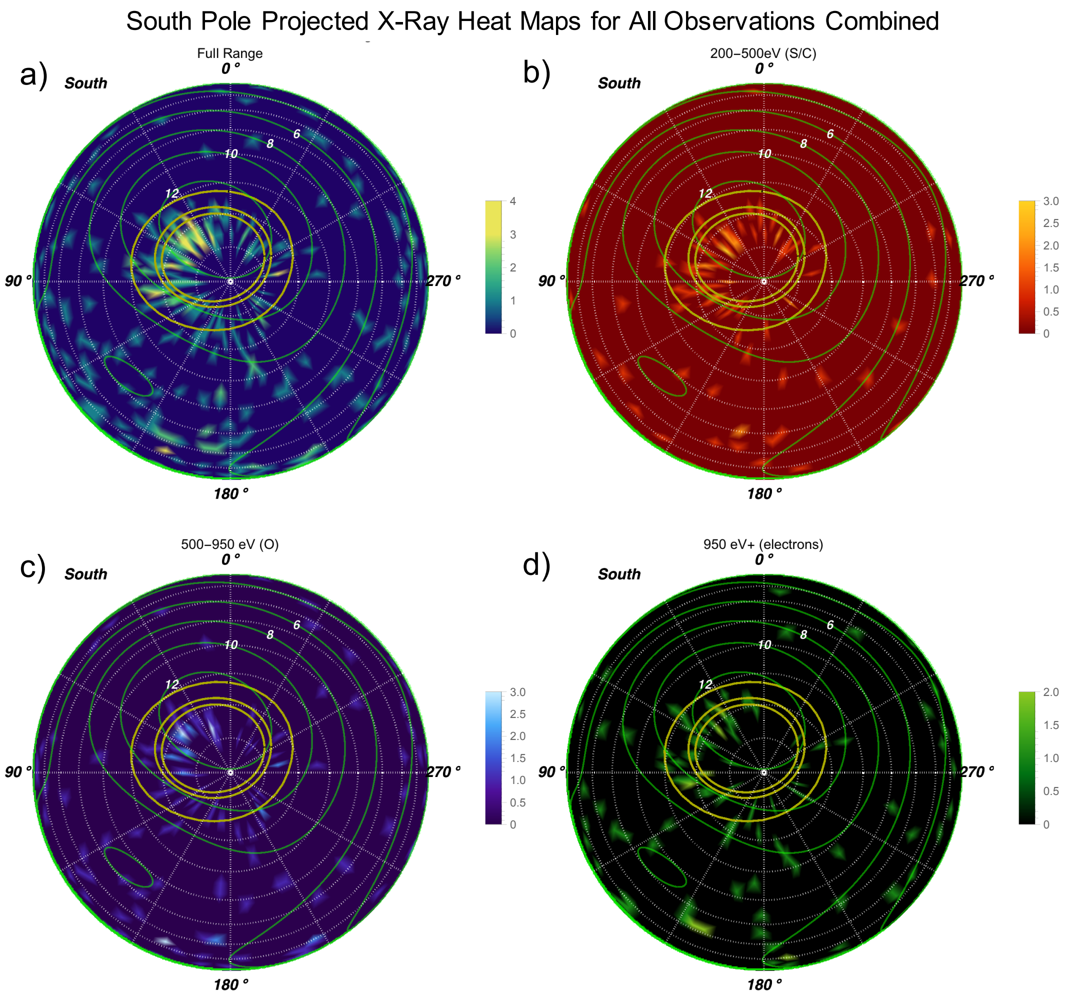

557 **Figure 10.** Projected X-ray heat maps centred on Jupiter's South pole from Chandra
558 ACIS observations. These show a) the full energy range in blue-green-yellow b) 0.2 0.5 keV
559 (sulphur/carbon emission) in red-yellow c) 0.5-0.9 keV (oxygen emission) in blue-white and
560 d) greater than 1 keV emission (hard X-ray bremsstrahlung from electron precipitation) in
561 green-yellow. The colour bar indicates the number of X-rays in bins of 4° by 4° of S3 latitude-
562 longitude. Dashed lines of longitude radiate from the pole, increasing anti-clockwise in increments
563 of 30° from 0° at the top. For further details see Fig. 9.

ferent parts of Solar Cycle 24, in good agreement with the strong evidence for the disk emission being predominately from scattered solar photons [*Bhardwaj et al.*, 2005, 2006; *Cravens et al.*, 2006; *Branduardi-Raymont et al.*, 2007a]. *Branduardi-Raymont et al.* [2010] compare the GOES solar X-ray emission with the Jovian disk emission from a variety of observations during solar cycle 23, finding powers between 0.1-1 GW. We report very similar values of 0.2 GW at solar minimum and 0.76 GW at solar maximum in 2014. It is possible that this slightly reduced emission during solar maximum (relative to the values observed in solar cycle 23) relates to a lower number of Sun spots in cycle 24 (Fig. 1), since solar flares cause instantaneous dramatic increases in the X-ray power of Jupiter's equatorial region [e.g. *Dunn et al.* [2016]].

Here, we studied XMM-Newton observations of solar spectrum variation over one activity cycle. Instrument brightness constraints mean XMM-Newton is unable to observe the Sun directly. However, indirect XMM-Newton observations of the disk-integrated Solar spectrum are possible through its reflection from Jupiter. These may also provide useful reference points to help interpret XMM-Newton observations of other stars. X-ray telescope time is in high demand, so it is rare that exoplanets have X-ray observations of their parent stars at all and when these observations are conducted they are often 'one-off' observations, capturing a very limited phase of a parent star's activity cycle. A deeper understanding of how spectral signatures diagnose the phase of our own Sun's activity cycle could allow for constraints to be placed on the phase of other G-type star's activity cycles [*Brooks et al.*, 2017; *Favata et al.*, 2008; *Oláh et al.*, 2016], when only one-off observations exist. Associated X-ray irradiance from these stars may drive exoplanet atmospheric signatures such as the prevalence of certain molecules or clouds, so a detailed understanding of the star-planet relationship is key [e.g. reviews in *Branduardi-Raymont et al.* [2017]; *Wolk et al.* [2019]]. However, we note that there are still uncertainties for the phases of grand maxima or minima of other stars, which are difficult to diagnose in only a few decades of observations.

6.2 Chandra ACIS-XMM-Newton EPIC-pn Auroral Comparisons

We found that typically Chandra ACIS records lower normalised counts keV^{-1} sec^{-1} than XMM-Newton EPIC-pn in the range from 0.4-0.6 keV. From 0.6 keV upwards they are generally in agreement. Many previous papers have discussed the apparent reduction in Oxygen emission observed between 0.5-0.6 keV relative to expected photon production from theory and comet observations [*Elsner et al.*, 2005; *Kharchenko et al.*, 2008; *Hui et al.*, 2010; *Ozak et al.*, 2010]. This has needed to be accounted for in the Monte Carlo modelling of particle precipitation and has required the invoking of quenching of specific oxygen lines [*Kharchenko et al.*, 2008] or differing opacity requirements [*Ozak et al.*, 2010]. *Hui et al.* [2010] commented that this could be a temporal effect or a consequence of Chandra's lower energy resolution. Here, we show simultaneous Chandra ACIS and XMM-Newton EPIC-pn spectra and find that for every observation the 0.5-0.6 keV emission is reduced in the Chandra ACIS data relative to the XMM-Newton EPIC-pn spectra, which are closer to expectations from charge exchange models. We therefore argue that this is an ACIS instrumental effect rather than a signature of temporal variability. However, opacity effects or differing local acceleration (e.g. different localised potential drops due to differences in surface magnetic field strength) and associated quenching may still be required to explain the differences between the Northern and Southern aurora [e.g *Ozak et al.* [2010]; *Dunn et al.* [2017]]. We recommend use of XMM-Newton spectra for analysis of Jupiter's X-ray auroral spectral lines.

6.3 Ion Precipitation in the Polar Region

Previously, two approaches have been taken to fitting the XMM-Newton and Chandra ACIS spectra. The first is to produce a model based on a combination of independent Gaussian lines (e.g. *Branduardi-Raymont et al.* [2004, 2007b]; *Elsner et al.* [2005];

Dunn et al. [2016]). The second is to use Monte Carlo models of particle precipitation [*Kharchenko et al.*, 2008; *Hui et al.*, 2009, 2010; *Ozak et al.*, 2010; *Houston et al.*, 2018], calculate subsequent charge state distributions and the photon yields from these, then modulate this emission through atmospheric effects. *Hui et al.* [2009, 2010] provided a comprehensive fit to 3 XMM-Newton EPIC-pn spectra and 2 Chandra ACIS spectra from 2003 with these Monte Carlo charge exchange models. For XMM-Newton they found that 2 (28th April and 27-29th Nov) of the 3 observations were better fitted with sulphur+oxygen models, while 1 (25th Nov 2003) was better fitted with a carbon+oxygen model. For Chandra they found that both observations (24-25th and 25-26th Feb 2003) were better fitted by a sulphur+oxygen model. They note the importance of a spectral feature in the 425 to 475 eV range expected from carbon ions, which lead them to exclude carbon in many fits. We find that ACIS and EPIC-pn can disagree on the observed emission.

We find that the sulphur+oxygen models provide good fits to the spectra and retrieve S:O ion ratios of 0.4 to 1.3 (varying from observation-to-observation and with the physics of the chosen model). These are in surprisingly good agreement with the magnetospheric ratios measured in-situ. The JEDI instrument on the Juno spacecraft recorded S:O ratios of between 0.5-1.5 with a mean of 0.9 for a perijove pass during December 2016 [G. Clark, priv comms]. *Radioti et al.* [2005, 2006] provided measurements on the S:O ratio from the Galileo spacecraft and summarised the results from Ulysses, Voyager 1 and Voyager 2 ion population data, finding S:O ion ratios between 0.3 and 1.2, depending on spacecraft and with values decreasing with radial distance [*Krimigis et al.*, 1979; *Vogt et al.*, 1979a,b; *Hamilton et al.*, 1980, 1981; *Lanzerotti et al.*, 1992; *Krupp*, 1994; *Mauk et al.*, 1998; *Maclennan et al.*, 2001; *Waldrop*, 2004]. This agreement suggests that most X-ray auroral emissions are produced by precipitating magnetospheric ions. *Mauk et al.* [2004] also show varying S:O ratios with radial distance, so it may be that changing S:O ratios in the auroral emission are indicative of changing seed ion populations in the magnetosphere and possibly a changing mapping location in the magnetosphere.

Comparing S:O ratios between the X-ray aurorae spectral fits and in-situ measurements may provide clues as to the drivers of Jupiter's X-ray aurorae. In general, there are likely to be at least two key factors controlling Jupiter's soft X-ray aurora if the ions that produce it originate in the magnetosphere. These factors may be deeply interconnected or may be independent. The first factor is the acceleration of ions to the MeV energies required to sufficiently strip electrons, so that the ions can undergo the observed X-ray-producing charge exchange interactions. The second factor is a process that delivers the ions into the loss cone at the poles of the planet. A range of possible processes have been proposed for both mechanisms, and the drivers of Jupiter's X-ray aurora remain a topic of debate [e.g. Cravens et al. 2003; Bunce et al. 2004; Dunn et al. 2017; Manners et al. 2018]. Either of these factors may be capable of changing the S:O ratio from the ratios observed in the seed population at the magnetospheric equator.

For instance, significant potential drops have long been proposed as a possible acceleration process (also capable of changing the loss cone) for the X-ray aurora [Cravens et al. 2003], and have recently been discovered over the poles of Jupiter by Juno [Clark et al. 2017]. However, the S^{+}:S^{++} ratio is not the same as the O^{+}:O^{++} ratio. An ion with multiple charges will be more accelerated by a potential drop than a singly charged ion. This produces scenarios where, for instance, an initial O^{++} ion can be sufficiently accelerated to produce X-ray emission, while an O^{+} ion cannot. It may therefore be possible to observe an X-ray auroral S:O ratio that is different to that of the seed population, if the ions have been accelerated through a potential drop.

Alternatively, a pitch angle scattering process that delivers the ions to the loss cone may also depend on particle species. For example, if gyro-frequency resonance interactions play some role in pitch angle scattering the ions then this will also depend on the ions mass and charge. The mass ratio of S and O is only a factor of two. The gyrofrequencies for singly charged S and O therefore only differ by a factor of 2, and are prone to similar resonance interactions. The ion gyrofrequency also changes with charge state, so that for example S^{++} and O^{+} have the same gyrofrequency and would both resonate with the same wave. There exist a range of possible gyrofrequencies for the combination of different masses and charges of sulphur and oxygen so that some S and O ions will share resonance interactions, while others do not. Again, this may lead to changes in the S:O ratio observed in the X-ray aurora compared with that seen in the magnetosphere seed population.

This is a complex problem for which the analytical and numerical modelling is beyond the scope of this paper. However, further research on how different proposed drivers change the X-ray auroral S:O ratio away from the ratio found in the seed ion population would help to constrain or eliminate drivers of Jupiter's X-ray aurora. We therefore note that the variation in S:O ratios may provide important clues towards the predominance of different processes in producing X-ray aurorae.

In contrast with the common best fits of sulphur+oxygen, the 8-9 March 2007 observations suggest that the precipitating population may sometimes include additional O^{7+} and possibly carbon, amongst other yet to be characterised emissions between 0.4-0.5 keV, which may partially be the distinguishing carbon lines discussed by *Hui et al.* [2009, 2010]. O^{7+} is present in the solar wind and the next most prevalent heavy ion after oxygen is carbon. Charge exchange of the solar wind with the neutral atmosphere of comets produce significant carbon and oxygen X-ray emission [*Kharchenko and Dalgarno*, 2000; *Lisse et al.*, 2001; *Krasnopolsky et al.*, 2004; *Cravens*, 2002]. The soft X-ray aurora from ion precipitation has been suggested to correspond to Jupiter's downward current region [*Cravens et al.*, 2003]. It seems unlikely that the sulphur+oxygen population that precipitates throughout the other observations, and has been observed to precipitate in certain polar regions by Juno [*Clark et al.*, 2017; *Haggerty et al.*, 2017; *Szalay et al.*, 2017] switches off entirely for this observation, although the hard X-ray emission from the upward current is very dim at this time. There is also a significant challenge in explaining the X-ray emission through solar wind ions alone, since the solar wind densities are too low and require 1000s MA current systems to generate the required fluxes [e.g. *Cravens et al.* [2003]; *Bunce et al.* [2004]]. *Kimura et al.* [2016]; *Dunn et al.* [2016] both show that the precipitating ions originate from the outer magnetosphere and suggest an origin near the noon to dusk magnetopause. If the population in this region were to have additional solar wind ions injected into it then this increasingly mixed population may result in observed solar wind X-ray signatures in the spectrum. The possible driving processes for these changes in the observed auroral particle precipitations are explored in detail in the context of the solar wind conditions and observed UV and radio emissions from the planet in the companion paper [*Dunn et al.*, in review].

While the 'equivalent temperature' ACX model [*Smith et al.*, 2012, 2014] that we apply to the EPIC-pn Jovian aurorae spectra is not as comprehensive as the Monte Carlo ion precipitation models applied previously [e.g. *Kharchenko et al.* [2008]; *Ozak et al.* [2010]; *Houston et al.* [2018]], it does appear to provide good spectral fits. There will be differences in the structure and location of charge exchange spectral lines for a thermalised model compared with the non-thermal processes that truly occur during ion precipitation into Jupiter's atmosphere. The results presented here may suggest that the limitations of the spectral resolution of EPIC-pn (or Chandra ACIS) combined with the low signal from Jupiter (for at least these observations) allow these 'equivalent temperature' ACX models to provide a valuable qualitative tool for relative comparison between observations. These models will be less reliable when applied to higher spectral resolution observations such as those provided by XMM-Newton's RGS instrument. However, for comparing observations of Jupiter's aurora over short time scales (e.g. the $\sim$6 hours for which the Northern aurora is in view each Jupiter rotation) the sensitivity limits of RGS and low signal from Jupiter mean that too few photons are collected to allow for modelling of high resolution spectra. When integrating over many Jupiter rotations during bright auroral conditions (as shown in *Branduardi-Raymont et al.* [2007b]), RGS may be able to catalogue the differences between a Monte Carlo model and the ACX models applied here, but key information on shorter timescale auroral variability will be lost.

Recent work has suggested that there may sometimes be multiple sources for Jupiter's X-ray aurora [e.g. *Dunn et al.* [2017]]. Indeed, the polar projections presented here (Fig. 9 and 10) suggest that while the region connected to the UV aurora active region [e.g. *Elsner et al.* [2005]] is the dominant location for Jupiter's X-ray aurora (see *Dunn et al.* [in review] for further details), there may be sparse X-ray emission poleward of this in the UV auroral swirl region. One additional contribution to the X-ray aurora, which may explain this sparse poleward emission is that singly charged heavy ions in the magnetosphere could undergo charge exchange with ambient neutrals (e.g., with the extended neutral distributions associated with Io and Europa) to form energetic neutral atoms (ENAs). These particles are no longer bound by the magnetic field of Jupiter and essentially travel in all directions (preserving the momentum they had as ions). The ENAs that pass close enough to Jupiter's extended atmosphere can become stripped (e.g. *Bishop* [1996]), forming ions again. This process would cause ions to interact with nearly the whole atmosphere. However, in regions of very strong field-aligned potential drops, it is possible that these newly stripped ions can be accelerated to the MeV/amu energies that are needed for X-ray emissions. Candidate regions of acceleration include the UV swirl region, where JEDI has found indications of upward very narrow beams of MeV electrons [*Paranicas et al.*, 2018]. These beams may be tracers of processes involving currents or other electromagnetics but they support the idea of large field-aligned potential drops poleward of the UV main emission. However, this process is unlikely to explain the majority of the X-ray auroral emission, because it would need to be modulated regularly with time in order to explain the pulsing auroral behaviour [e.g. *Dunn et al.* [2017]].

7 Conclusion

We present X-ray observations of Jupiter during February and March 2007. We find that the equatorial emission is significantly dimmer during the 2007 solar minimum (0.2 GW) compared to solar maximum (0.76 GW). In contrast with the reduced disk emission, the X-ray aurora has comparably bright intervals at both solar minimum and maximum, suggesting that any solar cycle control that does exist is more nuanced. To explore the auroral relationship with solar activity, the companion paper compares solar wind variation with the X-ray auroral emissions [*Dunn et al.*, in review].

XMM-Newton and Chandra observations of the Sun are not possible due to brightness constraints on the instrument. Reflected solar emission from Jupiter therefore provides a monitor of X-ray signatures of the activity cycle of our local star.

We show the spatial distribution of Jupiter's different X-ray auroral components (sulphur/carbon, oxygen and electron emission) through 2007 and find that the hard X-ray emission is generally very dim and that the ion emission is much brighter and concentrated in the expected regions poleward of the main emission.

Comparing simultaneous Chandra ACIS and XMM-Newton EPIC-pn spectra shows that ACIS consistently under reports 0.45-0.6 keV auroral emission relative to XMM-Newton (after applying the respective instrument responses in xspec), suggesting that some previous adaptations to physical models may not be required [*Kharchenko et al.*, 2008; *Ozak et al.*, 2010]. From 0.6 keV upwards Chandra ACIS and XMM-Newton EPIC-pn are generally in good agreement.

We explored modeling the auroral spectra using AtomDB Charge Exchange spectral lines and found these could fit the data well (reduced χ^2 of 0.8-1.3) for every XMM-Newton observation. The fits for Chandra ACIS spectra were less good due to the under-recorded 0.5-0.6 keV emission. Purely sulphur+oxygen models, representative of a magnetospheric plasma originating at Io, provided excellent fits to all but one data set. These retrieved S:O ion ratios of between 0.4 to 1.3, which are in excellent agreement with S:O ratios of 0.3-1.5 reported for in-situ Jovian magnetosphere measurements by NASA's Juno spacecraft and previous missions [e.g. *Radioti et al.* [2005, 2006]]. This further evidences that Jupiter's auroral flares are produced by precipitation from the magnetosphere.

Comparing two examples of different spectral behaviour from 2007, we show that the bright emission on the 24-25th February 2007 was best fit by sulphur and oxygen. In contrast, an observation on 8-9th March 2007 was even brighter but carbon and oxygen provided a better fit for this interval, suggesting a solar wind ion population precipitated in this interval. The companion paper for this [*Dunn et al.*, in review]explores the solar wind conditions, alongside UV and radio emissions contemporaneous with this campaign to constrain the reasons for the changing auroral behaviour.

Acknowledgments

WRD would like to thank V. Kharchenko for his invaluable and highly informative conversations on ion precipitation at Jupiter. WRD would also like to thank the Vogt/Masters and Jackman/Paranicas ISSI team meetings, which initiated this project. During the course of this work, W.R.D. was supported by a Science and Technology Facilities Council (STFC) research grant to University College London (UCL), an SAO fellowship to Harvard-Smithsonian Centre for Astrophysics and by European Space Agency (ESA) contract no. 4000120752/17/NL/MH. LCR was funded by an STFC consolidated grant to Lancaster University (ST/R000816/1). C.M.J. is supported by STFC Ernest Rutherford Fellowship ST/L004399/1. Z. H. Y. acknowledges financial support from the Belgian Federal Science Policy Office (BELSPO) via the PRODEX Programme of ESA. EJB was supported by STFC grant ST/N000749/1 and a Royal Society Wolfson Research Merit Award. D.B. is funded under STFC consolidated grant number ST/S000240/1. Hinode is a Japanese mission developed and launched by ISAS/JAXA, with NAOJ as domestic partner and NASA and STFC (UK) as international partners. It is operated by these agencies in co-operation with ESA and NSC (Norway). The Chandra and XMM-Newton data presented here is publicly available through the Chandra and XMM-Newton science archives. We greatly thank the Chandra and XMM-Newton Projects for their support.

References

Arnaud, K. (1996), Xspec: The first ten years, in *Astronomical Data Analysis Software and Systems V*, vol. 101, p. 17.

Bhardwaj, A., G. Branduardi-Raymont, R. F. Elsner, G. R. Gladstone, G. Ramsay, P. Rodriguez, R. Soria, J. Waite, and T. E. Cravens (2005), Solar control on jupiter's equatorial x-ray emissions: 26–29 november 2003 xmm-newton observation, *Geophysical Research Letters*, *32*(3).

Bhardwaj, A., R. F. Elsner, G. R. Gladstone, J. H. Waite, G. Branduardi-Raymont, T. E. Cravens, and P. G. Ford (2006), Low-to middle-latitude x-ray emission from jupiter, *Journal of Geophysical Research: Space Physics (1978–2012)*, *111*(A11).

Bishop, J. (1996), Multiple charge exchange and ionization collisions within the ring current-geocorona-plasmasphere system: Generation of a secondary ring current on inner l shells, *Journal of Geophysical Research: Space Physics*, *101*(A8), 17,325–17,336.

Branduardi-Raymont, G., R. Elsner, G. Gladstone, G. Ramsay, P. Rodriguez, R. Soria, and J. Waite Jr (2004), First observation of jupiter by xmm-newton, *Astronomy & Astrophysics*, *424*(1), 331–337.

Branduardi-Raymont, G., A. Bhardwaj, R. Elsner, G. Gladstone, G. Ramsay, P. Rodriguez, R. Soria, J. Waite, and T. Cravens (2007a), Latest results on jovian disk x-rays from xmm-newton, *Planetary and Space Science*, *55*(9), 1126–1134.

Branduardi-Raymont, G., A. Bhardwaj, R. Elsner, G. Gladstone, G. Ramsay, P. Rodriguez, R. Soria, J. Waite, T. Cravens, et al. (2007b), A study of jupiter's aurorae with xmm-newton, *Astronomy & Astrophysics*, *463*(2), 761–774.

Branduardi-Raymont, G., R. F. Elsner, M. Galand, D. Grodent, T. Cravens, P. Ford, G. Gladstone, and J. Waite (2008), Spectral morphology of the x-ray emission from jupiter's aurorae, *Journal of Geophysical Research: Space Physics (1978–2012)*, *113*(A2).

Branduardi-Raymont, G., A. Bhardwaj, R. Elsner, and P. Rodriguez (2010), X-rays from saturn: a study with xmm-newton and chandra over the years 2002–05, *Astronomy & Astrophysics*, *510*, A73.

Branduardi-Raymont, G., W. R. Dunn, and S. Sciortino (2017), Future exoplanet research: Xuv (euv and x-ray) detection and characterization, *Handbook of Exoplanets*, pp. 1–20.

Brooks, D. H., D. Baker, L. van Driel-Gesztelyi, and H. P. Warren (2017), A solar cycle correlation of coronal element abundances in sun-as-a-star observations, *Nature communications*, *8*(1), 183.

Bunce, E., S. Cowley, and T. Yeoman (2004), Jovian cusp processes: Implications for the polar aurora, *Journal of Geophysical Research: Space Physics (1978–2012)*, *109*(A9).

Clark, G., B. Mauk, D. Haggerty, C. Paranicas, P. Kollmann, A. Rymer, E. Bunce, S. Cowley, D. Mitchell, G. Provan, et al. (2017), Energetic particle signatures of magnetic field-aligned potentials over jupiter's polar regions, *Geophysical Research Letters*, *44*(17), 8703–8711.

Connerney, J., M. Acuna, N. Ness, and T. Satoh (1998), New models of jupiter's magnetic field constrained by the io flux tube footprint, *Journal of Geophysical Research: Space Physics (1978–2012)*, *103*(A6), 11,929–11,939.

Cowley, S., and E. Bunce (2001), Origin of the main auroral oval in jupiter's coupled magnetosphere–ionosphere system, *Planetary and Space Science*, *49*(10), 1067–1088.

Cravens, T. (2002), X-ray emission from comets, *Science*, *296*(5570), 1042–1045.

Cravens, T., E. Howell, J. Waite, and G. Gladstone (1995), Auroral oxygen precipitation at jupiter, *Journal of Geophysical Research: Space Physics (1978–2012)*, *100*(A9), 17,153–17,161.

Cravens, T., J. Waite, T. Gombosi, N. Lugaz, G. Gladstone, B. Mauk, and R. MacDowall (2003), Implications of jovian x-ray emission for magnetosphere-ionosphere coupling, *Journal of Geophysical Research: Space Physics (1978–2012)*, *108*(A12).

Cravens, T., J. Clark, A. Bhardwaj, R. Elsner, J. Waite, A. Maurellis, G. Gladstone, and G. Branduardi-Raymont (2006), X-ray emission from the outer planets: Albedo for scattering and fluorescence of solar x rays, *Journal of Geophysical Research: Space Physics (1978–2012)*, *111*(A7).

Dunn, W., G. Branduardi-Raymont, L. Ray, C. Jackman, R. Kraft, R. Elsner, I. Rae, Z. Yao, M. Vogt, G. Jones, et al. (2017), The independent pulsations of jupiter's northern and southern x-ray auroras, *Nature Astronomy*, *1*(11), 758.

Dunn, W. R., G. Branduardi-Raymont, R. F. Elsner, M. F. Vogt, L. Lamy, P. G. Ford, A. J. Coates, G. R. Gladstone, C. M. Jackman, J. D. Nichols, et al. (2016), The impact of an icme on the jovian x-ray aurora, *Journal of Geophysical Research: Space Physics*, *121*(3), 2274–2307.

Dunn, W. R., R. Gray, A. Wibisono, S. V. Badman, G. Branduardi-Raymont, R. F. Elsner, G. R. Gladstone, R. Ebert, L. Lamy, C. Louis, P. Ford, A. Foster, C. Tao, L. Ray, Z. Yao, I. J. Rae, E. J. Bunce, P. Rodriguez, C. M. Jackman, G. Nicolaou, H. Elliott, and R. Kraft (in review), Jupiter's x-ray emission 2007 part 2: Comparisons with uv and radio emissions and in-situ solar wind measurements, *Journal of Geophysical Research: Space Physics*.

Elsner, R. F., N. Lugaz, J. Waite, T. Cravens, G. Gladstone, P. Ford, D. Grodent, A. Bhardwaj, R. MacDowall, M. Desch, et al. (2005), Simultaneous chandra x ray, hubble space telescope ultraviolet, and ulysses radio observations of jupiter's aurora, *Journal of Geophysical Research: Space Physics (1978–2012)*, *110*(A1).

Favata, F., G. Micela, S. Orlando, J. Schmitt, S. Sciortino, and J. Hall (2008), The x-ray cycle in the solar-type star hd 81809-xmm-newton observations and implications for the coronal structure, *Astronomy & Astrophysics*, *490*(3), 1121–1126.

Gladstone, G., J. Waite, D. Grodent, W. Lewis, F. Crary, R. F. Elsner, M. Weisskopf, T. Majeed, J.-M. Jahn, A. Bhardwaj, et al. (2002), A pulsating auroral x-ray hot spot on jupiter, *Nature*, *415*(6875), 1000–1003.

Gladstone, G. R., J. H. Waite, and W. S. Lewis (1998), Secular and local time dependence of jovian x ray emissions, *Journal of Geophysical Research: Planets (1991–2012)*, *103*(E9), 20,083–20,088.

Golub, L., E. Deluca, G. Austin, J. Bookbinder, D. Caldwell, P. Cheimets, J. Cirtain, M. Cosmo, P. Reid, A. Sette, et al. (2008), The x-ray telescope (xrt) for the hinode mission, in *The Hinode Mission*, pp. 27–50, Springer.

Grodent, D., B. Bonfond, J.-C. Gérard, A. Radioti, J. Gustin, J. T. Clarke, J. Nichols, and J. E. Connerney (2008), Auroral evidence of a localized magnetic anomaly in jupiter's northern hemisphere, *Journal of Geophysical Research: Space Physics (1978–2012)*, *113*(A9).

Guo, R., Z. Yao, Y. Wei, L. C. Ray, I. Rae, C. S. Arridge, A. Coates, P. Delamere, N. Sergis, P. Kollmann, et al. (2018a), Rotationally driven magnetic reconnection in saturn's dayside, *Nature Astronomy*, p. 1.

Guo, R., Z. Yao, N. Sergis, Y. Wei, D. Mitchell, E. Roussos, B. Palmaerts, W. Dunn, A. Radioti, L. C. Ray, et al. (2018b), Reconnection acceleration in saturn's dayside magnetodisk: A multicase study with cassini, *The Astrophysical Journal Letters*, *868*(2), L23.

Haggerty, D., B. Mauk, C. Paranicas, G. Clark, P. Kollmann, A. Rymer, S. Bolton, J. Connerney, and S. Levin (2017), Juno/jedi observations of 0.01 to¿ 10 mev energetic ions in the jovian auroral regions: Anticipating a source for polar x-ray emission, *Geophysical Research Letters*, *44*(13), 6476–6482.

Hamilton, D., G. Gloeckler, S. Krimigis, C. Bostrom, T. Armstrong, W. Axford, C. Fan, L. Lanzerotti, and D. Hunten (1980), Detection of energetic hydrogen molecules in jupiter's magnetosphere by voyager 2: Evidence for an ionospheric plasma source, *Geophysical Research Letters*, *7*(10), 813–816.

Hamilton, D., G. Gloeckler, S. Krimigis, and L. Lanzerotti (1981), Composition of nonthermal ions in the jovian magnetosphere, *Journal of Geophysical Research: Space Physics*, *86*(A10), 8301–8318.

Hill, T. (2001), The jovian auroral oval, *Journal of Geophysical Research: Space Physics (1978–2012)*, *106*(A5), 8101–8107.

Houston, S., N. Ozak, J. Young, T. Cravens, and D. Schultz (2018), Jovian auroral ion precipitation: Field-aligned currents and ultraviolet emissions, *Journal of Geophysical Research: Space Physics*, *123*(3), 2257–2273.

Hui, Y., D. R. Schultz, V. A. Kharchenko, P. C. Stancil, T. E. Cravens, C. M. Lisse, and A. Dalgarno (2009), The ion-induced charge-exchange x-ray emission of the jovian auroras: Magnetospheric or solar wind origin?, *The Astrophysical Journal Letters*, *702*(2), L158.

Hui, Y., D. R. Schultz, V. A. Kharchenko, A. Bhardwaj, G. Branduardi-Raymont, P. C. Stancil, T. E. Cravens, C. M. Lisse, and A. Dalgarno (2010), Comparative analysis and variability of the jovian x-ray spectra detected by the chandra and xmm-newton observatories, *Journal of Geophysical Research: Space Physics (1978–2012)*, *115*(A7).

Jackman, C., C. Knigge, D. Altamirano, R. Gladstone, W. Dunn, R. Elsner, R. Kraft, G. Branduardi-Raymont, and P. Ford (2018), Assessing quasiperiodicities in jovian x-ray emissions: Techniques and heritage survey, *Journal of Geophysical Research: Space Physics*, *123*(11), 9204–9221.

Kharchenko, V., and A. Dalgarno (2000), Spectra of cometary x rays induced by solar wind ions, *Journal of Geophysical Research: Space Physics (1978–2012)*, *105*(A8), 18,351–18,359.

Kharchenko, V., W. Liu, and A. Dalgarno (1998), X ray and euv emission spectra of oxygen ions precipitating into the jovian atmosphere, *Journal of Geophysical Research: Space Physics (1978–2012)*, *103*(A11), 26,687–26,698.

Kharchenko, V., M. Rigazio, A. Dalgarno, and V. Krasnopolsky (2003), Charge abundances of the solar wind ions inferred from cometary x-ray spectra, *The Astrophysical Journal Letters*, *585*(1), L73.

Kharchenko, V., A. Dalgarno, D. Schultz, and P. Stancil (2006), Ion emission spectra in the jovian x-ray aurora, *Geophysical research letters*, *33*(11).

Kharchenko, V., A. Bhardwaj, A. Dalgarno, D. R. Schultz, and P. C. Stancil (2008), Modeling spectra of the north and south jovian x-ray auroras, *Journal of Geophysical Research: Space Physics (1978–2012)*, *113*(A8).

Kimura, T., R. Kraft, R. Elsner, G. Branduardi-Raymont, G. Gladstone, C. Tao, K. Yoshioka, G. Murakami, A. Yamazaki, F. Tsuchiya, et al. (2016), Jupiter's x-ray and euv auroras monitored by chandra, xmm-newton, and hisaki satellite, *Journal of Geophysical Research: Space Physics*, *121*(3), 2308–2320.

Krasnopolsky, V. A., J. B. Greenwood, and P. C. Stancil (2004), X-ray and extreme ultraviolet emissions from comets, *Space Science Reviews*, *113*(3-4), 271–373.

Krimigis, S., T. Armstrong, W. Axford, C. Bostrom, C. Fan, G. Gloeckler, L. Lanzerotti, E. Keath, R. Zwickl, J. Carbary, et al. (1979), Low-energy charged particle environment at jupiter: A first look, *Science*, *204*(4396), 998–1003.

Krupp, N. (1994), Drei-dimensionale richtungsverteilungen und relative häufigkeiten energiereicher ionen in der magnetosphäre des jupiter, Ph.D. thesis, Technische Universität Braunschweig.

Lanzerotti, L., T. Armstrong, R. Gold, K. Anderson, S. Krimigis, R. Lin, M. Pick, E. Roelof, E. Sarris, G. Simnett, et al. (1992), The hot plasma environment at jupiter- ulysses results, *Science*, *257*(5076), 1518–1524.

Lisse, C., D. Christian, K. Dennerl, K. Meech, R. Petre, H. Weaver, and S. Wolk (2001), Charge exchange-induced x-ray emission from comet c/1999 s4 (linear), *Science*, *292*(5520), 1343–1348.

Maclennan, C., L. Lanzerotti, and A. Lagg (2001), Hot plasma heavy ion abundance in the inner jovian magnetosphere (¡ 10 rj), *Planetary and Space Science*, *49*(3-4), 275–282.

Manners, H., A. Masters, and J. Yates (2018), Standing alfvén waves in jupiter's magnetosphere as a source of 10-to 60-min quasiperiodic pulsations, *Geophysical Research Letters*, *45*(17), 8746–8754.

Mauk, B., R. McEntire, D. Williams, A. Lagg, E. Roelof, S. Krimigis, T. Armstrong, T. Fritz, L. Lanzerotti, J. Roederer, et al. (1998), Galileo-measured depletion of near-io hot ring current plasmas since the voyager epoch, *Journal of Geophysical Research: Space Physics*, *103*(A3), 4715–4722.

Mauk, B., D. Mitchell, R. McEntire, C. Paranicas, E. Roelof, D. Williams, S. Krimigis, and A. Lagg (2004), Energetic ion characteristics and neutral gas interactions in jupiter's magnetosphere, *Journal of Geophysical Research: Space Physics*, *109*(A9).

Oláh, K., Z. Kővári, K. Petrovay, W. Soon, S. Baliunas, Z. Kolláth, and K. Vida (2016), Magnetic cycles at different ages of stars, *Astronomy & Astrophysics*, *590*, A133.

Ozak, N., D. R. Schultz, T. Cravens, V. Kharchenko, and Y.-W. Hui (2010), Auroral x-ray emission at jupiter: Depth effects, *Journal of Geophysical Research: Space Physics (1978–2012)*, *115*(A11).

Ozak, N., T. Cravens, and D. Schultz (2013), Auroral ion precipitation at jupiter: Predictions for juno, *Geophysical Research Letters*, *40*(16), 4144–4148.

Paranicas, C., B. Mauk, D. Haggerty, G. Clark, P. Kollmann, A. Rymer, B. Bonfond, W. Dunn, R. Ebert, G. Gladstone, et al. (2018), Intervals of intense energetic electron beams over jupiter's poles, *Journal of Geophysical Research: Space Physics*, *123*(3), 1989–1999.

Radioti, A., N. Krupp, J. Woch, A. Lagg, K.-H. Glassmeier, and L. Waldrop (2005), Ion abundance ratios in the jovian magnetosphere, *Journal of Geophysical Research: Space Physics*, *110*(A7).

Radioti, A., N. Krupp, J. Woch, A. Lagg, K.-H. Glassmeier, and L. Waldrop (2006), Correction to "ion abundance ratios in the jovian magnetosphere", *Journal of Geophysical Research: Space Physics*, *111*(A10).

Smith, R., A. Foster, and N. Brickhouse (2012), Approximating the x-ray spectrum emitted from astrophysical charge exchange, *Astronomische Nachrichten*, *333*(4), 301–304.

Smith, R. K., N. S. Brickhouse, D. A. Liedahl, and J. C. Raymond (2001), Collisional plasma models with apec/aped: emission-line diagnostics of hydrogen-like and helium-like ions, *The Astrophysical Journal Letters*, *556*(2), L91.

Smith, R. K., A. R. Foster, R. J. Edgar, and N. S. Brickhouse (2014), Resolving the origin of the diffuse soft x-ray background, *The Astrophysical Journal*, *787*(1), 77.

Szalay, J., F. Allegrini, F. Bagenal, S. Bolton, G. Clark, J. Connerney, L. Dougherty, R. Ebert, D. Gershman, W. Kurth, et al. (2017), Plasma measurements in the jovian polar region with juno/jade, *Geophysical Research Letters*, *44*(14), 7122–7130.

Vogt, M. F., M. G. Kivelson, K. K. Khurana, R. J. Walker, B. Bonfond, D. Grodent, and A. Radioti (2011), Improved mapping of jupiter's auroral features to magnetospheric sources, *Journal of Geophysical Research: Space Physics (1978–2012)*, *116*(A3).

Vogt, M. F., E. J. Bunce, M. G. Kivelson, K. K. Khurana, R. J. Walker, A. Radioti, B. Bonfond, and D. Grodent (2015), Magnetosphere-ionosphere mapping at jupiter: Quantifying the effects of using different internal field models, *Journal of Geophysical Research: Space Physics*.

Vogt, R., W. Cook, A. Cummings, T. Garrard, N. Gehrels, E. Stone, J. Trainor, A. Schardt, T. Conlon, N. Lal, et al. (1979a), Voyager 1: Energetic ions and electrons in the jovian magnetosphere, *Science*, *204*(4396), 1003–1007.

Vogt, R., A. Cummings, T. Garrard, N. Gehrels, E. Stone, J. Trainor, A. Schardt, T. Conlon, and F. McDonald (1979b), Voyager 2: Energetic ions and electrons in the jovian magnetosphere, *Science*, *206*(4421), 984–987.

Von Steiger, R., N. Schwadron, L. Fisk, J. Geiss, G. Gloeckler, S. Hefti, B. Wilken, R. Wimmer-Schweingruber, and T. Zurbuchen (2000), Composition of quasi-stationary solar wind flows from ulysses/solar wind ion composition spectrometer, *Journal of Geophysical Research: Space Physics*, *105*(A12), 27,217–27,238.

Waite, J., F. Bagenal, F. Seward, C. Na, G. Gladstone, T. Cravens, K. Hurley, J. Clarke, R. Elsner, and S. Stern (1994), Rosat observations of the jupiter aurora, *Journal of Geophysical Research: Space Physics (1978–2012)*, *99*(A8), 14,799–14,809.

Waite, J., G. Gladstone, K. Franke, W. Lewis, A. Fabian, W. Brandt, C. Na, F. Haberl, J. Clarke, K. Hurley, et al. (1995), Rosat observations of x-ray emissions from jupiter during the impact of comet shoemaker-levy 9, *SCIENCE-NEW YORK THEN WASHINGTON-*, pp. 1598–1598.

Waite, J., G. Gladstone, W. Lewis, P. Drossart, T. Cravens, A. Maurellis, B. Mauk, and S. Miller (1997), Equatorial x-ray emissions: Implications for jupiter's high exospheric temperatures, *Science*, *276*(5309), 104–108.

Waldrop, L. S. (2004), Probing the structure, composition, and dynamics of the jovian plasma sheet with energetic particles.

Wolk, S. J., J. J. Drake, G. Branduardi-Raymont, K. Poppenhaeger, V. Airapetian, K. France, S. Sciortino, I. Pillitteri, R. A. Osten, C. M. Lisse, et al. (2019), X-ray studies of exoplanets: A 2020 decadal survey white paper, *arXiv preprint arXiv:1904.04320*.

Yao, Z., A. Coates, L. Ray, I. Rae, D. Grodent, G. H. Jones, M. Dougherty, C. Owen, R. Guo, W. Dunn, et al. (2017), Corotating magnetic reconnection site in saturn's magnetosphere, *The Astrophysical Journal Letters*, *846*(2), L25.